



**HAL**  
open science

## The role of evaporites in the formation of gems during metamorphism of carbonate platforms: a review

Gaston Guiliani, Jean Dubessy, Daniel Ohnenstetter, David Banks, Yannick Branquet, Julien Feneyrol, Anthony E. Fallick, Jean-Emmanuel Martelat

### ► To cite this version:

Gaston Guiliani, Jean Dubessy, Daniel Ohnenstetter, David Banks, Yannick Branquet, et al.. The role of evaporites in the formation of gems during metamorphism of carbonate platforms: a review. *Mineralium Deposita*, 2018, 53 (1), pp.1-20. 10.1007/s00126-017-0738-4 . insu-01528349

**HAL Id: insu-01528349**

**<https://insu.hal.science/insu-01528349>**

Submitted on 28 Nov 2019

**HAL** is a multi-disciplinary open access archive for the deposit and dissemination of scientific research documents, whether they are published or not. The documents may come from teaching and research institutions in France or abroad, or from public or private research centers.

L'archive ouverte pluridisciplinaire **HAL**, est destinée au dépôt et à la diffusion de documents scientifiques de niveau recherche, publiés ou non, émanant des établissements d'enseignement et de recherche français ou étrangers, des laboratoires publics ou privés.

# Mineralium Deposita

## The role of evaporites in the formation of gems during metamorphism of carbonate platforms: a review --Manuscript Draft--

<b>Manuscript Number:</b>	
<b>Full Title:</b>	The role of evaporites in the formation of gems during metamorphism of carbonate platforms: a review
<b>Article Type:</b>	Regular Articles
<b>Corresponding Author:</b>	Gaston Giuliani, PhD. CRPG/CNRS Vandoeuvre, Meurthe et Moselle FRANCE
<b>Corresponding Author Secondary Information:</b>	
<b>Corresponding Author's Institution:</b>	CRPG/CNRS
<b>Corresponding Author's Secondary Institution:</b>	
<b>First Author:</b>	Gaston Giuliani, PhD.
<b>First Author Secondary Information:</b>	
<b>Order of Authors:</b>	Gaston Giuliani, PhD. jean Dubessy, PhD. Daniel Ohnenstetter, PhD. David Banks, PhD. Yannick Branquet, PhD. Julien Feneyrol, PhD. Anthony Fallick, PhD. Jean-Emmanuel Martelat, PhD.
<b>Order of Authors Secondary Information:</b>	
<b>Funding Information:</b>	Département Soutien et Formation, Institut de Recherche pour le Développement   Dr. Gaston Giuliani
<b>Abstract:</b>	The mineral and fluid inclusions trapped by gemstones during the metamorphism of rocks in carbonate platform successions are precious markers for the understanding of the gem genesis. The nature and chemical composition of inclusions highlight the major contribution of evaporites through dissolution or fusion, depending on the temperature of formation from the greenschist to the granulite facies. The fluids are highly saline NaCl-brines circulating either in an open system in the greenschist facies (Colombian and Afghan emeralds) and with huge fluid-rock metasomatic interactions, or sulphurous fluids (ruby, garnet tsavorite, zoisite tanzanite and lapis-lazuli) or molten salts formed in a closed system with a low fluid mobility (ruby in marble) in the conditions of the amphibolite to granulite facies. These chloride-fluoride-sulphate ± carbonate-rich fluids scavenged the metals essential for the gem formation. At high temperature, anions SO <sub>4</sub> <sup>2-</sup> , NO <sub>3</sub> <sup>-</sup> , BO <sub>3</sub> <sup>-</sup> and F <sup>-</sup> which are powerful fluxes lowered the temperature of chlorine and fluoride ionic liquids. They provided transport over a very short distance of aluminium, and/or silica and transition metals which are necessary for gem growth. So, the genetic models proposed for these high-value and ornamental gems underline the importance of the metamorphism of evaporites formed on carbonate continental shelves, and emphasises the chemical power accompanying the metamorphism at moderate to high temperatures of these particular evaporite-rich and organic matter-rich protoliths to form gem minerals.
<b>Suggested Reviewers:</b>	Bernd Lehmann, PhD.

Editor Mineralium Deposita, Technical University of Clausthal  
lehmann@min.tu-clausthal.de  
Dr. Bernd Lehmann, Editor of Mineralium Deposita, who invited us to write this paper on the role of evaporites in the formation of metamorphic gems, published in a short version as "Le fluide, l'Arlésienne du métamorphisme" in the Journal Géochronique, N°136, décembre 2015 entitled "Regards croisés sur le métamorphisme".

Georges beaudoin, PhD.  
professor, Université Laval  
Georges.Beaudoin@ggl.ulaval.ca  
As an Editor of Mineralium Deposita, Journal who invites our group to submit the present ms.  
Dr. Beaudoin participated to the bank of PhD. thesis of Julien Feneyrol one of the authors. He knows well the gem thematic

Robert Linnen, PhD.  
Professor, Western University  
r.linnen@uwo.ca  
geochemist specialist of fluids who has experience and knowledge in gems formation

1  
2  
3  
4  
5  
6  
7  
8  
9  
10  
11  
12  
13  
14  
15  
16  
17  
18  
19  
20  
21  
22  
23  
24  
25  
26  
27  
28  
29  
30  
31  
32  
33

**The role of evaporites in the formation of gems during metamorphism  
of carbonate platforms: a review**

Gaston Giuliani<sup>1,2</sup>, Jean Dubessy<sup>3</sup>, Daniel Ohnenstetter<sup>4</sup>, David Banks<sup>5</sup>, Yannick Branquet<sup>6,7</sup>,  
Julien Feneysel<sup>8</sup>, Anthony E. Fallick<sup>9</sup>, Jean-Emmanuel Martelat<sup>10</sup>

1- Université Paul Sabatier, GET/IRD, UMR CNRS-IRD-CNRS 5563, 14 avenue Edouard  
Belin, 31400 Toulouse, France

2- Université de Lorraine, CRPG UMR 7358 CNRS-UL, 15 rue Notre-Dame-des-Pauvres,  
BP 20, 54501 Vandœuvre-lès-Nancy cedex, France

3- Université de Lorraine, GeoRessources UMR 7359 CNRS-UL, BP 70239, 54506  
Vandœuvre-lès-Nancy, France

4- 4 rue Nicolas Chopin, 88130 Marainville-sur-Madon, France

5- University of Leeds, School of Earth and Environment, Woodhouse Lane, Leeds LS2 9JT,  
United Kingdom

6- ISTO, UMR 7327-CNRS/Université d'Orléans/BRGM, 1A rue de la Férollerie, 45071  
Orléans cedex 2, France

7- Géosciences-Rennes, UMR6881-CNRS/Université de Rennes I, Campus de Beaulieu,  
35042 Rennes Cedex, France

8- Arethuse Geology, Latitude Arbois, 1060 Rue René Descartes, 13290 Les Milles, France

9- Isotope Geosciences Unit, S.U.E.R.C., Rankine Avenue, East Kilbride, Glasgow G75  
0QF, Scotland, United Kingdom

10- Laboratoire de Géologie de Lyon (LGLTPE), Université de Lyon 1, ENSL, UMR 5276, 2  
rue Raphaël Dubois, Géode, 69622 Villeurbanne Cedex, France

34  
35  
36  
37  
38  
39  
40  
41  
42  
43  
44  
45  
46  
47  
48  
49  
50  
51  
52  
53  
54  
55  
56  
57  
58  
59  
60  
61  
62  
63  
64  
65  
66

**Abstract** The mineral and fluid inclusions trapped by gemstones during the metamorphism of rocks in carbonate platform successions are precious markers for the understanding of the gem genesis. The nature and chemical composition of inclusions highlight the major contribution of evaporites through dissolution or fusion, depending on the temperature of formation from the greenschist to the granulite facies. The fluids are highly saline NaCl-brines circulating either in an open system in the greenschist facies (Colombian and Afghan emeralds) and with huge fluid-rock metasomatic interactions, or sulphurous fluids (ruby, garnet tsavorite, zoisite tanzanite and lapis-lazuli) or molten salts formed in a closed system with a low fluid mobility (ruby in marble) in the conditions of the amphibolite to granulite facies. These chloride-fluoride-sulphate  $\pm$  carbonate-rich fluids scavenged the metals essential for the gem formation. At high temperature, anions  $\text{SO}_4^{2-}$ ,  $\text{NO}_3^-$ ,  $\text{BO}_3^-$  and  $\text{F}^-$  which are powerful fluxes lowered the temperature of chlorine and fluoride ionic liquids. They provided transport over a very short distance of aluminium, and/or silica and transition metals which are necessary for gem growth. So, the genetic models proposed for these high-value and ornamental gems underline the importance of the metamorphism of evaporites formed on carbonate continental shelves, and emphasises the chemical power accompanying the metamorphism at moderate to high temperatures of these particular evaporite-rich and organic matter-rich protoliths to form gem minerals.

**Keywords**

67 gems, emerald, ruby, garnet, zoisite, lapis-lazuli, metamorphism, carbonate platform,  
68 evaporites, brines, fingerprints, salinity, molten salts, thermal reduction of sulphates

## 69 **Introduction**

70 The classical quality-grading criteria for gems are based on clarity, colour, carat and cut.  
71 These 4 “C” criteria are dependent on the geological, physical and chemical conditions  
72 existing during the gem growth. The formation of coloured gems necessitates the existence of  
73 four conditions: (1) a parental fluid issued either from the gem host-rock environment or  
74 exotic fluid circulations; (2) a seed surface and sufficient space for the growth of the crystal;  
75 (3) the incorporation of trace elements from the parental fluid in the unit cell of the mineral;  
76 and (4) the absence of internal crystalline deformation during and after growth.

77 The colour and transparency will make the difference between a mineralogical specimen  
78 and a gem. The chromophores are mostly transition metals such as Ti, V, Cr, Mn, Fe, Cu  
79 which have approximately the same atomic radius as the substituted major element(s) of the  
80 mineral. On the other hand, the exceptional optical quality of gemstones make them an object  
81 of choice for the study of solid and fluid inclusions (FI) trapped during their growth, and these  
82 are sometimes excellent geological and/or geographical fingerprints (Giuliani et al. 2014a).

83 This paper is focused on metamorphic gems and ornamental gemstones such as  
84 Colombian and Afghan emeralds, ruby-bearing marbles in central and south-east Asia, garnet  
85 vanadium-rich grossular i.e. tsavorite and vanadium-rich zoisite called tanzanite from  
86 Tanzania, Kenya and Madagascar, and lapis-lazuli in marble and/or calc-silicate rocks from  
87 Afghanistan (Fig. 1). Previous studies highlighted special common features: (i) the presence  
88 of halite, sulphates and minerals rich in Cl, Na, Mg, B and F; and (ii) either the trapping of  
89 high-salinity aqueous ( $\pm$  carbonic) FI or CO<sub>2</sub>-H<sub>2</sub>S-S<sub>8</sub>-rich FI (Roedder 1963; Giuliani et al.  
90 1993a; Giuliani et al. 2003; Garnier et al. 2008; Feneyrol et al. 2013; Giuliani et al. 2015a).  
91 Three questions arise concerning these metamorphic gems primarily due to change in the  
92 conditions of heat and pressure, and fluid-rock interactions by diffusion or percolation  
93 (metasomatism): (1) the origin and the role of these fluids; (2) the nature and the importance  
94 of the protolith; and (3) the characteristics of the paleogeography of the depositional  
95 sedimentary environment. During this review, we will show the efficiency of different  
96 analytical techniques which allow the acquisition of relevant data for answering these  
97 questions.

98

## 99 **The geological setting of metamorphic gems**

100

101 Recent petrographical and geochemical data obtained on the formation of metamorphic  
102 deposits such as Colombian and Afghan emeralds, Asian ruby-bearing marbles, tsavorite and  
103 tanzanite in East Africa (Groat 2014), and lapis-lazuli of Sar-e-Sang in Afghanistan (Faryad  
104 2002), allowed the characterization of the protoliths of these gem-bearing metamorphic rocks.  
105 These are calcareous benches alternating with black shales (BS), initially rich in organic  
106 matter (OM), with intercalation of levels of evaporitic rocks. The latter are not recognizable  
107 after metamorphism as such, but mineralogy and paleofluids contained in primary fluid  
108 inclusions witness their past presence (Giuliani et al. 2003).

109

### 110 **Colombian emerald deposits**

111 Located in the Eastern Cordillera basin, the Colombian emerald deposits define two belts: the  
112 eastern belt encompassing the mining districts of Gachalá, Chivor and Macanal, and the  
113 western belt including the mining districts of Yacopi, Muzo, Coscuez, La Pita and Peñas  
114 Blancas (Fig. 2A). Emerald mineralisation is hosted in the Lower Cretaceous sedimentary  
115 series characterized by a succession of sandstone, limestone, black shale (BS), and evaporites  
116 (Fig. 3). Detailed structural mapping and geometric analysis provided evidence that emerald  
117 mineralisation is associated to structural events drastically different between the western and  
118 eastern belts (Branquet et al. 1999a). The Muzo and Coscuez deposits are linked to tear faults  
119 and associated thrusts during a compressive tectonic event whereas the eastern emerald  
120 deposits, such as that of Chivor, present extensional structures extending from a brecciated  
121 evaporitic level which acted as a local, gravity-driven detachment. These tectonic structures  
122 are both synchronous with the circulation of hydrothermal fluids and emerald formation. The  
123 fluid-rock interaction processes led to Na and Ca metasomatism of the enclosing carbonated  
124 carbon-rich BS. Leaching of major (K, Al, Si, Ti, Mg, P), trace (Be, Cr, V, Rb, Sc, U, C) and  
125 REE elements from the BS is accompanied by their partial redistribution to minerals in the in-  
126 filling vein system, especially Cr and V which are incorporated in emerald (Giuliani et al.  
127 1993b). Emerald formed at a temperature (T) ~ 300-330°C and a pressure (P) ~ 0.5-1.2 kbar  
128 which correspond to a depth about 4 to 5 km (Cheilletz et al. 1994; Ottaway et al. 1994).

129 The eastern emerald belt: the Chivor mines

130 The mines are scattered along a regional white-brecciated evaporitic unit which contains  
131 emerald veins (Fig. 2B). The brecciated rock unit in the Chivor area, which is in excess of 10  
132 km long and 10 m thick (Figs. 4A, B), is stratiform, i.e. parallel to the sedimentary strata, and  
133 dominantly composed of a breccia (Fig. 4C) made up of fragments from the hanging wall

134 (carbonated carbon-rich BS, limestone and whitish albitite, i.e. an albitised BS) cemented by  
135 carbonates and pyrite (Fig. 4D). Its formation is related to the dissolution of an evaporitic  
136 horizon (Branquet et al. 2015). All the mineralized structures extend vertically from the  
137 brecciated level. In the Chivor mines, emerald is located in cm- to dm-thick carbonate-pyrite-  
138 bearing (Fig. 1A) listric faults, meter-wide extensional fractures injected with hydrothermal  
139 breccia, and extensional sets of fractures in the albitite (Fig. 4E) and calcareous carbon-rich  
140 BS of the Macanal Formation. The brecciated level, the hydrothermal fluid circulation and  
141 emerald formation occurred at  $65 \pm 3$ Ma (Cheilletz et al. 1997).

142 The western emerald zone: the Muzo and Coscuez mining districts

143 On the western side, the deposits are hectometer-sized at most and display numerous folds,  
144 thrusts and tear faults (Fig. 5; Laumonier et al. 1996; Branquet et al. 1999a). At the Muzo  
145 deposit, thrusts are characterized by the carbonated BS which overlie siliceous BS (Fig. 6).  
146 All the tectonic contacts are marked by cm- to m-thick hydrothermal breccias called by the  
147 local miners "cenicero", i.e. ashtray (generally, well delimited white coloured zone which has  
148 the aspect of ash during the dry season). These white- or red-coloured breccias outline the  
149 thrust planes, which are associated with intense hydraulic fracturing (Branquet et al. 1999b).  
150 Multistage brecciation corresponds to successive fault-fluid flow pulses, and dilatant sites  
151 resulting from shear-fracturing synchronous to the thrust fault propagation. Each pulse is  
152 associated with: (i) emerald-bearing banded carbonate vein-like structures present throughout  
153 the breccia; (ii) emerald-bearing thrust-associated carbonate veins occurring in the wall rocks  
154 and composed of calcareous BS called "cama" by the local miners (emerald zone forming a  
155 layer which is parallel to the thrust fault); and (iii) emerald-bearing carbonate veins initiating  
156 in the breccia zone and crosscutting the wall-rocks. All of these tectonic structures are  
157 associated with fluid circulation in the calcareous carbon-rich BS which induced intense  
158 albitisation, carbonatisation and pyritisation. The siliceous BS called "cambiado"(zones which  
159 have changed by comparison with the cama) by the local miners have no mineralisation.

160 At the Coscuez deposit, the folds and thrusts were guided by the Coscuez tear fault which  
161 acted as a vertical conduit for the mineralizing fluids developed in the carbonated carbon-rich  
162 BS. Hydraulic breccias (Fig. 7), formed by the opening of dilatant sites related to fluid over-  
163 pressures and hydrothermal replacement, are similar to those described for the Muzo deposit.  
164 The genesis of the deposit is the consequence of a compressive phase characterized by folding  
165 and thrusting along tear faults formed at the Eocene-Oligocene boundary (Cheilletz et al.  
166 1994) and associated with fluid overpressure. These complex structures are probably linked to

167 a basal regional décollement or detachment fault thought to be at the level of the evaporites  
168 (Branquet et al. 1999a, b).

169 At the regional scale, the presence of sedimentary levels with gypsum, residues of dissolution  
170 of salts (called "rute" by Colombian miners) in the Lower Cretaceous series of the Eastern  
171 Cordillera and saliferous diapirs, confirm that the continental shelf series is saliferous. The  
172 significant albitisation of the BS and precipitation of albite in the hydrothermal veins  
173 (Branquet et al. 1999a) testifies to important brine circulations. Furthermore, at the Chivor  
174 mines, the presence in the upper albitites (see Fig. 4A) of coalescent replacement of anhydrite  
175 nodules into carbonates, tepee and enterolithic structures argue for the evaporitic origin of the  
176 protolith (Branquet et al. 2015).

177

### 178 **Emerald deposits from Afghanistan**

179 The main commercial emerald deposits are centred on the Panjshir Valley, 230 km NW of  
180 Kohistan (Bowersox et al. 1991; Fig. 8). The valley coincides with the Herat-Panjshir strike-  
181 slip fault which was active in the Oligo-Miocene (Tapponnier et al. 1981). The emerald  
182 deposits, located on the southeastern part of the Panjshir fault zone, are dated, by Ar-Ar  
183 technique on micas, at  $23 \pm 1$  Ma (Sabot et al. 2000). The Kendjt, Khalat and Gujari deposits  
184 are located along the shear zone cutting Palaeozoic metasedimentary rocks formed by  
185 intercalations of schist, dolomitic marble and quartzite, in the upper greenschist facies (Kazmi  
186 and Snee 1989; Vapnik and Moroz 2001). Emerald is confined to quartz-ankerite-dolomite-  
187 pyrite veinlets and veins linked to shear zones (Fig. 1C). The metasomatic alteration due to  
188 the fluid circulation resulted in the phlogopitisation, albitisation and silicification of the wall-  
189 rocks. Albitites resembling those of Colombia are described by Sabot et al. (2000). The  
190 metasomatic minerals include dravite tourmaline, pyrite, albite and phlogopite. The origin of  
191 chromium, vanadium and beryllium is unknown because there are no reported whole-rock  
192 analysis of the emerald-hosting metamorphic formations.

193

### 194 **Ruby and lapis-lazuli from central and south-east Asia**

195 Ruby in marble deposits

196 One of the main worldwide sources for excellent-quality ruby with intense colour and high  
197 transparency (Fig. 1D) is associated with marble deposits from central and south-east Asia  
198 (Hughes 1997). The deposits occur in Afghanistan, Pakistan, Azad-Kashmir, Tajikistan,  
199 Nepal, Myanmar, northern Vietnam and southern China (Garnier et al. 2008; Fig. 8). These

200 deposits are found in metamorphosed platform carbonates associated generally with marbles  
201 intercalated with garnet-biotite-sillimanite- or biotite-kyanite-bearing gneisses which are  
202 sometimes intruded by granitoids (Pêcher et al. 2002). The marble units consist of  
203 discontinuous horizons up to 300 m in thickness, oriented parallel to the main regional  
204 foliations, thrusts or shear zones related to the Cenozoic Himalayan orogenesis between 45  
205 and 5 Ma (Garnier et al. 2006). The ruby mineralisation is restricted to peculiar impure  
206 marble horizons. The protolith of the ruby-bearing metamorphic rocks comprises carbonates  
207 enriched in detrital clays and organic matter (OM), and intercalated evaporitic layers (Fig. 3).  
208 Ruby crystals occur: (i) disseminated within marbles and associated with phlogopite,  
209 muscovite, scapolite, margarite, spinel, titanite, pyrite and graphite, as in Jegdalek,  
210 Afghanistan; Chumar and Ruyil, Nepal; Hunza and Nangimali, Pakistan; Mogok and Mong  
211 Hsu, Myanmar; and Luc Yen, Vietnam; (ii) in veinlets or gash veins, as in some occurrences  
212 in northern Vietnam, and associated with phlogopite, margarite, titanite, graphite and pyrite,  
213 and sometimes related to micro-shear zones, as in Nangimali in Pakistan; (iii) in pockets  
214 associated with orthoclase, phlogopite, margarite, graphite and pyrite in some occurrences of  
215 northern Vietnam. Gem ruby formed during the retrograde metamorphism stage at  $T \sim 620-$   
216  $670^{\circ}\text{C}$  and  $P \sim 2.6-3.3$  kbar (Garnier et al. 2008). The aluminium and the chromophorous  
217 elements of ruby originate from the marbles (Al up to 1000 ppm, V and Cr between 5 to 30  
218 ppm).

219

#### 220 Lapis-lazuli deposits

221 The antique and famous ornamental lapis-lazuli deposits at Sar-e-Sang in the north-eastern  
222 part of Afghanistan (Fig. 8) occur within the high-grade metamorphic rocks of the Goran  
223 series. U-Pb, K-Ar and Rb-Sr radiometric data gave a minimum Proterozoic age at 2.13 Ga  
224 for the amphibolite facies metamorphism of the Goran series (Russian literature cited in  
225 Hubbard et al. 1999) while  $^{40}\text{Ar}/^{39}\text{Ar}$  ages of micas associated with micaschist and phlogopite  
226 from ultramagnesian rocks gave a range of ages, from 17 to 22 Ma, indicative of a Miocene  
227 cooling age due to Himalayan exhumation activity (Hubbard et al. 1999). The lapis-lazuli  
228 formed lenses or layers in calcite and dolomite marbles containing fine lenses or more thicker  
229 anhydrite levels (Kulke 1974) and white schists (Kulke and Schreyer 1973) intercalated with  
230 calc-silicate rocks, amphibolites and quartzites, and occur also at the contact between granite  
231 or pegmatite with marble (Faryad 2002). The thickness of the lenses and layers is between 2  
232 to 6 m while the extension is between 40 to 450 m. Generally, the central part of the layers  
233 formed by calcite-diopside-lazurite (Fig. 1F) is bordered, on one side, by a diopside-rich zone

234 (40 to 90 vol. %), and on the other side by a phlogopite-diopside-calc-silicate rock zone (with  
235 also scapolite, tremolite, zoisite, epidote). P-T conditions of metamorphism are  $T \sim 750^{\circ}\text{C}$   
236 and  $P \sim 13\text{-}14$  kbar (Faryad 2002).

237

### 238 **Garnet tsavorite and zoisite tanzanite in East Africa**

239 All tsavorite deposits are hosted in the Neoproterozoic Metamorphic Mozambique Belt  
240 (NMMB) stretching from the Arabian-Nubian shield to East Antarctica, through East Africa,  
241 Madagascar and Pakistan (Feneyrol et al. 2013). The economic deposits are found in Kenya,  
242 Tanzania and Madagascar (Fig. 9). They formed during Neoproterozoic Himalayan-type  
243 continental collision between eastern and western Gondwana blocks, between 650 and 550  
244 Ma, following the complex closure of the Mozambique Ocean. Tsavorite is hosted by a  
245 metasedimentary sequence (Fig. 3) formed by a succession of quartzite, kyanite  $\pm$  sillimanite-  
246 biotite  $\pm$  almandine graphitic gneiss, graphitic gneiss with intercalations of calc-silicate rock,  
247 meta-evaporite and marble (Olivier 2006; Feneyrol et al. 2010). The calc-silicate rocks in the  
248 graphitic gneisses display enterolithic structures (Figs. 10B, C) and  $\pm$  anhydrite-diopside and  
249 tsavorite nodules (Figs. 10A, D; Feneyrol et al. 2013).

250 Tsavorite is mined within primary deposits either as nodules (Type I) or in quartz veins (Type  
251 II), and placers (Type III):

252 (i) Type I: the nodules (Fig. 1E) and meta-evaporite levels are stratiform and occur among  
253 calc-silicates and graphitic gneisses such as in the Kenyan tsavorite belt (Fig. 9C; Fig. 10A).  
254 The tsavorite-bearing nodules are scattered in the Ca-rich rocks and formed through  
255 metamorphic reactions between calcareous beds or concretionary lenses and sulphate-rich  
256 levels intercalated within carbon-rich shale (Fig. 10A). The nodules formed during prograde  
257 metamorphism and tsavorite formed upon anhydrite or barite at  $T \sim 580\text{-}690^{\circ}\text{C}$  and  $P \sim 5\text{-}7$   
258 kbar (Feneyrol et al. 2013).

259 In the deposits from Kenya, Tanzania and Madagascar, V and Cr contents of graphitic  
260 gneisses are respectively up to 3600 ppm and 900 ppm (Fig. 3). In Tanzania, for the Merelani  
261 deposit (Fig. 9C), the source of V for tsavorite is apparently graphite hosted by the graphitic  
262 gneiss, which has a V content up to 2600 ppm indicating that original OM was V-rich (Olivier  
263 2006). In the Lemshuku deposit (Fig. 9C), the graphite associated with the gneiss and calc-  
264 silicate rocks has no V and Cr but the V and Cr contents of the graphite-bearing gneisses are  
265 respectively, between 200 and 2000 ppm, and 60 and 300 ppm (Feneyrol 2012). The V and Cr  
266 precursors have been consumed during the prograde metamorphism to form V and Cr-bearing  
267 kyanite, graphite, muscovite, rutile, diopside, titanite or karelianite.

268 (ii) Type II: deformation played an important role in the mineralizing processes for the quartz  
269 vein deposits found in Tanzania (Merelani and Ruangwa deposits; Figs. 9A, C). Vein  
270 formation and hydrothermal-metasomatic fluid circulation (carbonatisation, pyritisation and  
271 graphitisation) affecting the graphitic gneisses and calc-silicates were coeval with regional  
272 metamorphism (Feneyrol et al. 2013). Tsavorite in veins and pockets (Fig. 1G) formed during  
273 the retrograde stage at T 505-590°C and P ~ 3.6-4.9 kbar. Gem tanzanite at Merelani (Fig.  
274 1H) formed later in pockets and lenses at T ~ 385-450°C and P ~ 2.2 and 3.6 kbar (Feneyrol  
275 2012). It is associated with low grade metamorphic assemblages with commonly prehnite, ( $\pm$   
276 quartz) and calcium zeolites (chabazite, heulandite, mesolite, laumontite), axinite and blue  
277 apatite (Wilson et al. 2009).

278

279 In conclusion, gems mentioned in this study formed during the metamorphism of sedimentary  
280 carbonate platform formations containing evaporitic rocks from Neoproterozoic to Cenozoic  
281 time, and at temperatures between 300 and 750°C. The question arises as to the nature of the  
282 gem protolith and the geochemistry of the fluids. In the next section, we will focus on detailed  
283 aspects showing the importance of evaporites in the formation of these gems and their  
284 associated paragenesis.

285

## 286 **The mineral and geochemical fingerprints of the past presence of evaporites**

287

### 288 Mineralogy

289

290 In the Colombian deposits, crystals of anhydrite, halite and sometimes sylvite are trapped by  
291 emerald, quartz, albite and pyrite (Giuliani et al. 1993a).

292 In the ruby deposits, variations of local chemistry of the protolith along several decimetres are  
293 due to lateral facies variations which resulted in a succession of different paragenesis: (1) F-  
294 aspidolite (sodic phlogopite with Na<sub>2</sub>O between 6.2 and 6.6 wt. %, K<sub>2</sub>O between 0.4 and 0.6  
295 wt. %, and MgO between 25.8 and 26 wt. %) associated with F-phlogopite and F-paragonite  
296 in the different mineralized zones of ruby, as evidenced in the Nangimali deposit in Pakistan  
297 (Garnier et al. 2004); (2) anhydrite either associated with F-tremolite, - edenite, - pargasite,  
298 and calcite in samples from the Hunza Valley, Pakistan, and Luc Yen, Vietnam, or included  
299 in ruby with relics of spinel (Fig. 11A); (3) anhydrite and salt crystals (CaCl<sub>2</sub>, NaCl and KCl)  
300 as solid inclusions (Figs. 11C to E) in most of the rubies observed by SEM method, as in

301 Nangimali and Luc Yen deposits (Garnier et al. 2008), and (4) F-bearing minerals such as  
302 dravite-uvite tourmaline and apatite indicating a low activity of water in the fluid.

303 In the tsavorite and tanzanite deposits, the presence of different metamorphic mineral  
304 associations results from lateral facies variations of the initial protolith. Tsavorite from the  
305 deposit of Namalulu in Tanzania, is associated with F-Na-Cl-SO<sub>4</sub>-Li-rich minerals that  
306 indicate the presence of rich precursor evaporite-bearing sediments in the protolith (Feneyrol  
307 et al. 2012): (i) the Na-Ca-Cl-scapolites with Na<sub>2</sub>O between 6.5 and 7.9 wt. % and Cl between  
308 2.3 and 2.8 wt. % as well as F-tremolite (F up to 3.8 wt. %); (ii) anhydrite crystals associated  
309 with F-tremolite and dolomite in lenses in dolomitic marble (Fig. 11F); (iii) F-rich titanite  
310 with very high F-content (1 to 1.6 wt. % F) as well as phlogopite (2 to 4.8 wt. % F); (iv) the  
311 nodules of tsavorite concentrate towards their periphery F-bearing minerals with high F<sup>-</sup>/OH<sup>-</sup>  
312 ratio such as F-phlogopite (Fig. 10D) and F-apatite, testifying again to a low activity of water  
313 in the fluid and a strong fluoride activity; and (v) tsavorite is associated with a rare mineral  
314 described for the first time in the metamorphic environment (Feneyrol et al. 2012): the F-  
315 tainiolite (Fig. 11G) {KLiMg<sub>2</sub>(Si<sub>4</sub>O<sub>10</sub>)(F,OH)} which contains 8.9 to 9.4 wt. % F, 2 wt. %  
316 LiO<sub>2</sub>, and between 50 and 110 ppm of boron. Tainiolite is associated with a F-tremolite  
317 containing 3.5 wt. % F and up to 730 ppm of lithium. Additionally, barite is observed in the  
318 nodules of tsavorite at the Nadan 1 mine in Kenya (Fig. 11B).

319 At Sar-e-Sang lapis-lazuli deposit, scapolite and halogen-bearing minerals formed during  
320 prograde metamorphism of carbonate-evaporite sequences: (i) scapolite with Na<sub>2</sub>O between  
321 3.8 and 12.4 wt. % and Cl between 0.3 and 4.2 wt. %; (ii) sodalite close to the ideal end-  
322 member Na<sub>4</sub>Al<sub>6</sub>Si<sub>6</sub>O<sub>12</sub>Cl; (iii) h uyne and lazurite with compositions respectively,  
323 Ca<sub>1.2</sub>Al<sub>6</sub>Si<sub>6</sub>Cl<sub>0.2</sub>O<sub>29</sub> and Na<sub>5.5</sub>Ca<sub>0.9</sub>Al<sub>5.8</sub>Si<sub>6</sub>Cl<sub>0.1</sub>O<sub>29</sub>; (iv) F-phlogopite (F ~ 1 to 3.4 wt. %); (v)  
324 Na-amphibole (F-Cl-pargasite and edenite with Cl ~ 1.1 and 1.7 wt. % Cl); (vi) F-Cl-apatite  
325 containing chlorine up to 6.8 wt% and fluorine up to 4.8 wt. % (Faryad 2002). The presence  
326 of Na-Cl-scapolite implies an evaporitic source with NaCl provided by salt-rich layers  
327 (Faryad 2002). Besides, the magnesian kyanite-sillimanite-cordierite-dravite talcschists  
328 associated with these lazurite-bearing marbles result also from the metamorphism of  
329 evaporites (Schreyer and Abraham 1976). The dravite contains around 2.6 wt. % Na<sub>2</sub>O and  
330 0.1 to 0.13 wt. % F.

331

332 In conclusion, all these gemstones contain F (excepted Colombian emeralds), Cl, Li, Na, Mg  
333 and B mineralogical markers which testify to the importance played by the intercalations of

334 evaporitic levels in the sedimentary series which were subsequently metamorphosed during  
335 orogenesis. For the Colombian emeralds, the circulation of chlorine and sodium brines in the  
336 décollement zones of the basin, responsible for the albitisation of the BS coeval with emerald  
337 formation, characterised the end of the subsidence of the basin which was associated with the  
338 first tectonic-metamorphic episode affecting the eastern border of the Eastern Cordillera  
339 basin. The second tectonic phase reactivated similar fluid circulation processes on the western  
340 border. In both borders, the process for crystallisation of emerald took place in an open  
341 hydrothermal-metamorphic system. In Afghanistan, the absence of detailed geology and  
342 petrography of the deposits precludes any comprehensive genetic hypothesis, but the emerald  
343 veins are related to shear zones and fluid circulation led to the albitisation of the schists.  
344 For the other gems, the marbles or the gneisses contained intercalations of calc-silicate rocks  
345 and meta-evaporites. The chemical reactions are strongly spatially limited to the nodules  
346 and/or to the lenses of evaporites, which is evidence of a very low fluid circulation. The  
347 formation of ruby, tsavorite, tanzanite and lapis-lazuli occurred in quasi-closed systems.

348

#### 349 **Geochemistry of the paleo-fluids**

350 Paleo-fluids trapped as primary FI in the minerals during their growth allow accession to the  
351 composition of the mineralising fluids. Different techniques are used for their characterisation  
352 such as microthermometry, Raman and infrared spectrometries, crushing of FI for analysis of  
353 the cations and anions, and analysis of noble gases (Samson et al. 2003). The combination of  
354 these data with those obtained on the stable isotope ratios of elements such as oxygen,  
355 hydrogen, sulphur and boron on minerals coeval with the gems, permits the characterization  
356 of the origin and source of the different chemical elements.

#### 357 Colombian emerald

358 Fluids trapped by emerald are commonly three-phase FI (Fig. 12A) characterized by the  
359 presence of a daughter mineral, i.e. halite (NaCl). At room temperature, the cavities contain  
360 75 vol. % of salty water, i.e. an aqueous brine (liquid H<sub>2</sub>O), 10 vol. % of gas corresponding to  
361 the vapour bubble (V), and 15 vol. % of halite daughter mineral (H). However, some  
362 Colombian emeralds have multiphase FI presenting a liquid carbonic phase (CO<sub>2</sub>) forming up  
363 to 3 vol. % of the total cavity volume (Figs. 3A, 12B), minute crystals of calcite (Fig. 12A),  
364 very rare liquid and gaseous hydrocarbons (Kozłowski et al. 1988), and sometimes two or  
365 three cubes of halite (Figs. 12A, 12B), and sylvite (KCl). These H<sub>2</sub>O-NaCl±CO<sub>2</sub>-(Ca-K-Mg-  
366 Fe-Li-SO<sub>4</sub>) fluids (Banks et al. 2000) are NaCl saturated (~ 40 wt% eq. NaCl) and were

367 trapped at  $T \sim 300\text{-}330^\circ\text{C}$  (Roedder 1963; Giuliani et al. 1993a; Cheilletz et al. 1994; Ottaway  
368 et al. 1994). The high Cl/Br ratio of the fluids (between 6,300 and 18,900) indicates that the  
369 strong salinity of the brines derived from dissolution of halite of evaporitic origin (Fig. 13A;  
370 Banks et al. 2000). Cation exchanges, especially calcium, with the BS host rocks are strong  
371 when compared to most basinal and bittern fluids (Yardley and Bodnar 2014) and due to the  
372 relatively high temperature of the parent brines of emerald. Indeed, these fluids are enriched  
373 in Ca (16,000 to 32,000 ppm), base metals (Fe  $\sim$ 5,000 to 11,000 ppm; Pb  $\sim$ 125-230 ppm; Zn  
374  $\sim$ 170-360 ppm), lithium (Li  $\sim$ 400-4300 ppm) and sulphates ( $\text{SO}_4 \sim$ 400-500 ppm).  
375 Nevertheless there is no fluorine in these fluids (Table 1). As comparison, they have a  
376 composition and Fe/Cl and Cl/Br ratio (Table 1) similar to the fluids of the geothermal system  
377 of Salton Sea in California (Fig. 13B; Yardley and Cleverley 2013). The K/Na ratios confirm  
378 the Na-rich character of the fluids and the strong disequilibrium between K-feldspar and  
379 albite, as illustrated by the huge albitisation of the BS (Fig. 14).

380 The isotopic composition of the oxygen ( $\delta^{18}\text{O}$ ) of  $\text{H}_2\text{O}$  in equilibrium with Colombian  
381 emerald, calculated at  $300^\circ\text{C}$ , are higher ( $15.5 < \delta^{18}\text{O} < 17.1$  ‰ for the eastern belt, and  $17.5$   
382  $< \delta^{18}\text{O} < 23.6$  ‰ for the western belt; Giuliani et al. 2000) than those of classical basinal  
383 waters which have lower temperatures of formation. Besides, the range of values of isotopic  
384 composition of sulphur ( $\delta^{34}\text{S}$ ) of pyrite associated with emerald (Fig. 1A) corresponds to the  
385 isotopic range of values for sulphates (marine anhydrite) of the Lower Cretaceous of  
386 Colombia (Giuliani et al. 1995).

#### 387 Afghan emerald

388 Primary multiphase halite-sylvite-bearing FI (Fig. 12C) are common for the Panjshir emeralds  
389 (Kazmi and Snee 1989; Giuliani et al. 1997). The fluids associated with emerald precipitation  
390 have total dissolved salts (TDS) between 300 and 370 g/l and the trapping temperature of the  
391 fluid is about  $400^\circ\text{C}$  (Vapnik and Moroz 2001).

392 Crush-leach analyses of the electrolyte chemistry of fluid inclusions are presented in Table  
393 1. The fluids are Cl-Na-rich and they contain sulphates ( $140 < \text{SO}_4 < 4,300$  ppm) and lithium  
394 ( $170 < \text{Li} < 260$  ppm) but very low to zero fluorine contents (Table 1). The K/Na ratio of the  
395 fluid inclusions confirms the disequilibrium, at  $\sim 400^\circ\text{C}$ , between K-feldspar and albite which  
396 drives the Na-metasomatism of the metamorphic schists and the deposition of albite in the  
397 veins (Fig. 14). Crushing demonstrates that fluids are dominated by NaCl with Cl/Br ratios  
398 much greater than that of seawater (Fig. 13A), indicating that the salinity was derived by  
399 dissolution of halite. Thus the high Cl/Br ratios are consistent with halite dissolution for the

400 origin of salinity. The diagram I/Cl versus Br/Cl (Fig. 13B) shows also that the fluid  
401 inclusions have low I contents that are also typical of brines derived from evaporite  
402 dissolution. They compare with Hansonburg and contemporary fluids from the Salton Sea  
403 geothermal brines (Fig. 13B), both of which have dissolved evaporites (Williams and  
404 McKibben 1989; Bolkhe and Irwin 1992).

#### 405 Ruby in marble

406 Microthermometry studies combined with Raman spectroscopy of primary FI trapped by ruby  
407 indicate the contemporary trapping of two types of carbonic FI (Giuliani et al. 2015a): mono-  
408 to two-phase FI (Fig. 3) in the system  $\text{CO}_2\text{-H}_2\text{S-(}\pm\text{ COS } \pm\text{ S}_8) \pm (\text{H}_2\text{O, } < 10 \text{ mol. \%})$  and  
409 polycrystalline FI (Fig. 12D) in the system  $(\text{Na-K-Ca-CO}_3\text{-SO}_4\text{-NO}_3\text{-Cl-F}) \pm (\text{CO}_2\text{-}$   
410  $\text{H}_2\text{S}) \pm (\text{H}_2\text{O})$ . The different solids in the polycrystalline FI are mixtures of carbonates with  
411 Ca-Na-Al cations, such as shortite and dawsonite, sulphates - mainly anhydrite and barite,  
412 phosphates (F-apatite), nitrates, fluorides (fluorite), and chlorides (halite, Ca and K chlorides).  
413 These solids are daughter minerals (Fig. 12D) of ionic liquids formed during the  
414 metamorphism of evaporites and limestones (Giuliani et al. 2015a). As comparison, the  
415 polycrystalline inclusions represent for ruby the product of crystallization of molten salts,  
416 while for granites they are interpreted as the products of crystallization of silicate melts. In  
417 ruby, these polycrystalline FI are rare because if the salts are not immediately trapped by the  
418 crystals they are removed due to their strong solubility in water-rich fluids.

419 Crushing and leaching of rubies (Giuliani et al. 2015a) have shown that chloride is the  
420 dominant anion (25 to 53 mol. %) followed by sulphate (2 to 36 mol. %), nitrate (2 to 17  
421 mol. %) and fluoride (0 to 25 mol. %). Sodium is the dominant cation (16 to 42 mol. %). The  
422 Li contents are very low (0.3 to 9 mol. %). The presence of nitrate, detected by both Raman  
423 spectroscopy and crush-leach techniques, is a strong argument for a continental input to the  
424 original sediment as, generally, nitrate salts precipitate in closed basin playas or salars  
425 (Ericksen 1983). In addition, the isotopic variation of sulphur of the anhydrites included in  
426 ruby and marble defines two sets of  $\delta^{34}\text{S}$  values: the first, between 27 and 23 ‰, for a marine  
427 anhydrite; the second, between 4.8 and 1.6‰, for a continental source (Garnier et al. 2008).

#### 428 Tsavorite and Tanzanite

429 The primary FI trapped by both minerals belong to the  $\text{H}_2\text{S-S}_8 (\pm \text{N}_2 \pm \text{CH}_4)$  system (Fig.  
430 12E). Crush-leach analyses of tsavorite have shown that sulphate is the dominant anion (up to  
431 50 mol. %) while lithium is absent and fluoride is very low (0 to 4 mol. %; unpublished data).  
432 SIMS in situ analyses of dravite tourmaline associated with nodules of tsavorite from Kenya,

433 Tanzania and Madagascar (Fig. 15) showed similar isotopic compositions of  $\delta^{11}\text{B} = -19.8 \pm$   
 434  $1.2\text{‰}$  (n= 7). The range of boron isotopic composition ( $-20 < \delta^{11}\text{B} < -18.5 \text{‰}$ ; Giuliani et al.  
 435 2015b) clearly indicates continental evaporitic materials and confirms the genetic model  
 436 proposed for the formation of tsavorite in the metasedimentary series of the NMMB (Feneyrol  
 437 et al. 2013). The sediments were derived from an ancient platform in a widespread and  
 438 shallow evaporite-bearing epi-epireic platform with alternation of marine and non-marine  
 439 seaways on the border of the Mozambican Ocean.

#### 440 Lapis-lazuli

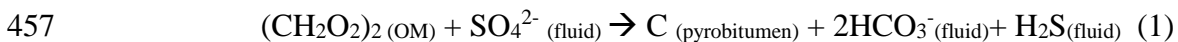
441 Up to now the observations on the paragenesis associated with lapis-lazuli have not revealed  
 442 the presence of cavities of FI or polycrystalline inclusions. Different minerals formed during  
 443 the prograde and retrograde metamorphic stages. At peak P-T metamorphism, the presence of  
 444 scapolite with diopside, grossular, calcite and quartz implies high  $\text{CO}_2$  and NaCl  
 445 concentrations in the fluid phases ( $X_{\text{CO}_2} = 0.03\text{-}0.15$  and  $X_{\text{NaCl}}$  between 0.04 and 0.99; Faryad  
 446 2002). During the retrograde stage, lazurite precipitated with sodalite, haüyne,  $\text{F}^-$  or  $\text{Cl}^-$ -rich  
 447 apatite, amphibole, scapolite, clinohumite and sometimes biotite.

448

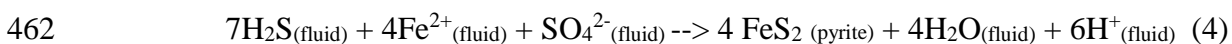
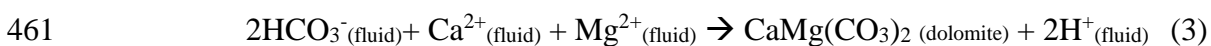
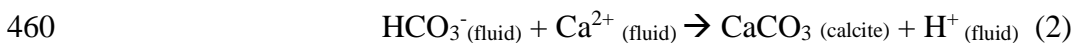
#### 449 Discussion on the role of evaporites in the formation of metamorphic gems

450

451 Parental brines of Colombian emeralds are responsible for the albitisation of the BS. They are  
 452 at the origin of the mobilisation, under the form of chlorine and fluoride complexes, of  
 453 aluminium, beryllium (Wood 1992), chromium (Vasin et al. 2004), vanadium (Povolov et al.  
 454 2007) and iron present in the BS. Sulphates are very sensitive to the conditions of thermal  
 455 reduction, and in the presence of OM, the sulphate is reduced to sulphide (Machel et al.  
 456 1995), and OM is oxidized to  $\text{CO}_2$  and then transformed into  $\text{HCO}_3^-$ :

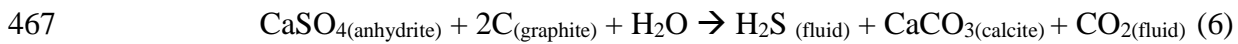
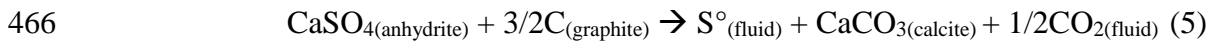


458 Products of this thermal reduction of sulphate in the presence of OM are involved in the  
 459 formation of carbonates and sulphides (Giuliani et al. 2000):



463

464 In the case of ruby hosted in marble, these redox reactions are also proposed to explain the  
 465 association of pyrite and calcite with ruby (Giuliani et al. 2003):



469 These reactions explain : (i) the involvement of anhydrite in these reactions, i.e. the presence  
470 of anhydrite crystals included in ruby and in marble shows that the reaction progress was not  
471 achieved to completion; (ii) the formation of CO<sub>2</sub> by oxidation of organic matter under  
472 graphitisation and/or graphite; (iii) the formations of native sulphur (reaction 5); (iv) the  
473 consumption of H<sub>2</sub>O (reaction 6); and (v) the formation of COS gas in the primary fluid  
474 (reaction 7), a rare component in geological fluids, that implies H<sub>2</sub>O-poor fluids.

475 The presence of SO<sub>4</sub><sup>2-</sup>, NO<sub>3</sub><sup>-</sup>, CO<sub>3</sub><sup>2-</sup>, BO<sub>3</sub><sup>-</sup> and F<sup>-</sup> decreased consequently the temperature of  
476 melting of halite and other salts, and allowed the formation of chlorine and fluorine-bearing  
477 ionic liquids. The fluorine of continental origin probably played an important role in the  
478 extraction of the aluminium present in the impurities (clays) of the impure limestone. For  
479 comparison, the fluorine and aluminate-rich flux method is used by industry for the  
480 production of Al by electrolysis due to the formation of AlF<sup>4-</sup> complexes (e.g. Lacassagne et  
481 al. 2002). So, the existence of an ionic liquid trapped in the form of polycrystalline solids by  
482 the ruby explains the colour and clarity of the ruby by: (i) the mobilization of Al, Cr and V  
483 contained in the metamorphosed limestone (Al ~ 1 000 ppm, Cr and V ~5 to 30 ppm for the  
484 Nangimali deposit in Pakistan); and (ii) their incorporation in an isotropic and fluid  
485 environment allowing crystalline growth with a minimum of defects (Giuliani et al. 2015a).

486 For tsavorite and tanzanite, the presence of anhydrite or barite in the tsavorite-bearing nodules  
487 as well as H<sub>2</sub>S-S<sub>8</sub>-bearing FI in tsavorite points out the importance of halite and sulphates in  
488 the gem formation. The notable quantity of F<sup>-</sup> and Cl<sup>-</sup> in phlogopite, titanite and scapolite  
489 associated with tsavorite, suggests that these elements have played a leading role in the  
490 mobilization of Al, and of V and Cr-bearing phengites and organic matter included in the  
491 anhydrite during the prograde metamorphism (Figs. 16B, 16C; Olivier 2006; Feneyrol et al.  
492 2013).

493 For lapis-lazuli, the reduction of sulphates (Faryad 2002), at T ~ 750°C and P ~ 13-14 kbar, in  
494 the upper amphibolite to granulite facies, played a key role in its formation since blue colour  
495 results from the absorption of visible light by the radical S<sup>3-</sup> present in its structure (Reinen  
496 and Lindner 1999). The radical S<sup>3-</sup> was highlighted recently experimentally in aqueous fluids  
497 (Pokrovski and Dubrovinsky 2011; Pokrovski and Dubessy 2014) and also those resulting

498 from the thermal reduction of sulphate (Truche et al. 2014). The evaporitic protolith  
499 associated with lapis-lazuli formed an almost anhydrous chemical system which suggests that  
500 the  $S^{3-}$  radical could be stable also in ionic liquids originating from the melting and thermal  
501 reduction of evaporites at high temperature.

502

503 The set of geological and geochemical data obtained on these different deposits confirms the  
504 presence in the protoliths of evaporites, of either continental or marine origin, which are  
505 considered as a key feature in the metamorphic model for these gems (Fig. 16). They would  
506 have formed during the metamorphism, from the greenschist to granulite facies, of carbonates  
507 interbedded with OM-bearing mudstones, and containing intercalations of sulphates-  
508 chlorides-nitrates-borates of impure evaporitic rocks. The lithological control of the  
509 mineralisation is essential. These particular sedimentary lithologies and the nature of the  
510 metamorphic piles permit the delineation of the paleogeography of the depositional  
511 sedimentary environment. The sedimentary landscape converged to an epeiric carbonate  
512 platform succession with a combination of saltern and evaporite mudflats of gypsum and  
513 anhydrite such as described by Warren (2006).

514 The separation of the pericontinental and epicontinental seaways implies the presence of a  
515 sedimentary or a tectonic barrier, and at times the shallow epeiric seaway was converted to  
516 saltern mudflat (sabkha) with continental inputs. The presence of carbonate or siliciclastic  
517 and/or evaporitic matrix in the rocks is indicative of sediment deposited in a continental zone  
518 which was temporarily flooded by the tides, such as proposed for ruby hosted in  
519 metasediments (Garnier et al. 2008). The marine coastal sabkha environment is characterized  
520 by the formation of gypsum and anhydrite crystals, and nodules typically with enterolithic and  
521 'chicken-wire' textures confirming their formation in supratidal zones such as described for  
522 the Colombian BS series and the Tanzanian and Kenyan metamorphosed BS formations. The  
523 high concentration of graphite in some metamorphic levels in the Kenyan Neoproterozoic  
524 tsavorite belt may represent original microbial mats (Feneyrol et al. 2013).

525

## 526 **Perspectives**

527

528 In spite of their differences in chemical composition, crystallisation system, physical  
529 conditions of metamorphism (P-T), scale of fluid circulation and ages, these metamorphic  
530 gemstones have in common a geochemical history connected to the nature of their mother  
531 protoliths.

532 Their mineralogical, chemical and isotopic characteristics are witnesses of fluid-rock  
533 interactions in open or closed systems. The understanding of their geological formation is one  
534 of the keys for the identification of their origin. The mineral and fluid inclusions trapped by  
535 gems during the metamorphism of rocks in carbonate platform successions are precious  
536 markers for understanding the genesis of the gems. The nature and chemical composition of  
537 the inclusions highlight the major contribution of evaporites by dissolution (for Colombian  
538 and Afghan emeralds) or melting (for other gems), depending of their temperature of  
539 formation. Solubility experiments of these gems in chloride-fluoride ionic liquids should be  
540 done together with speciation studies of the different chemical components involved in these  
541 minerals in order to generate thermodynamic models of such metamorphic ionic liquids.  
542 Other worldwide deposits such as lapis-lazuli in Myanmar, Russia and Baffin Island in  
543 Canada, emeralds from Davdar and Musakashi, respectively in China and Zambia,  
544 Precambrian sodalite from Bahia state in Brazil, lazulite in the Neoproterozoic Itremo  
545 quartzite from central Madagascar, now suggest investigation of the possible presence of  
546 evaporites in the formation of these high-value and ornamental gems. Guidelines for  
547 prospecting new gem deposits of metamorphosed carbonate platform-related areas worldwide  
548 include: (i) the lithological control of the mineralisation from an ancient platform evaporite  
549 environment with alternation of marine and non-marine seaways, i.e. a marine coastal sabkha-  
550 like environment; (ii) the presence of index minerals such as anhydrite, scapolite, aspidolite,  
551 and chloride-fluoride-sulphate  $\pm$  carbonate-rich fluid inclusions which can decipher the major  
552 contribution of evaporites by their dissolution or fusion, depending of their temperature of  
553 formation.

554

### 555 **Acknowledgements**

556 The authors would like to thank Dr. Bernd Lehmann, Editor of *Mineralium Deposita*, who  
557 invited us to write this paper on the role of evaporites in the formation of metamorphic gems,  
558 published in a short version as "Le fluide, l'Arlésienne du métamorphisme" in the *Journal*  
559 *Géochronique*, N°136, décembre 2015 entitled "Regards croisés sur le métamorphisme".

560

### 561 **References**

- 562 Banks D, Giuliani G, Yardley BWD, Cheilletz A (2000) Emerald mineralisation in Colombia:  
563 fluid chemistry and the role of brine mixing. *Miner Deposita* 35: 699-713  
564 Barth S (1993) Boron isotope variations in nature - a synthesis. *Geol Rundschau* 83: 640-651

565 Bohlke JK, Irwin JJ (1992) Laser microprobe analyses of Cl, Br, I and K in fluid inclusions -  
566 implications for sources of salinity in some ancient hydrothermal fluids. *Geochim*  
567 *Cosmochim Acta* 56: 203-225

568 Bowersox GW, Snee LW, Foord EF, Seal RRII (1991) Emeralds of the Panjshir Valley,  
569 Afghanistan. *Gems & Gemology* 27: 26-39

570 Branquet Y, Laumonier B, Cheilletz A, Giuliani G (1999a) Emeralds in the Eastern Cordillera  
571 of Colombia: Two tectonic settings for one mineralisation. *Geology* 27: 597-600

572 Branquet Y, Cheilletz A, Giuliani G, Laumonier B (1999b) Fluidized hydrothermal breccia in  
573 dilatant faults during thrusting: the Colombian emerald deposits. In: McCaffrey KJW,  
574 Lonergan L, Wilkinson JJ (eds) *Fractures, fluid Flow and Mineralisation*. Geological  
575 Society, London, United Kingdom, Special Publications, 155, pp 183-195

576 Branquet Y, Giuliani G, Cheilletz A, Laumonier B (2015) Colombian emeralds and  
577 evaporites: tectono-stratigraphic significance of a regional emerald-bearing evaporitic  
578 breccia level. In: André-Mayer AS, Cathelineau M, Muecher Ph, Picard E, Sindern S (eds)  
579 *From source, transport and metal deposits to mineral resources in a sustainable world*,  
580 *Proceedings of the 13th biennial meeting of the Society for Geology Applied to Mineral*  
581 *Deposits*, Nancy, France, pp 1291- 1294

582 Cheilletz A, Féraud G, Giuliani G, Rodriguez CT (1994) Time-pressure-temperature  
583 formation of Colombian emerald: an  $^{40}\text{Ar}/^{39}\text{Ar}$  laser-probe and fluid inclusion-  
584 microthermometry contribution. *Econ Geol* 89: 361-380

585 Cheilletz A, Giuliani G, Branquet Y, Laumonier B, Sanchez AJM, Féraud G, Arhan T (1997)  
586 Datation K-Ar et  $^{40}\text{Ar}/^{39}\text{Ar}$  à  $65 \pm 3$  Ma des gisements d'émeraude du district de Chivor-  
587 Macanal: argument en faveur d'une déformation précoce dans la Cordillère Orientale de  
588 Colombie. *C R Acad Sci* 324: 369-377

589 Ericksen GE (1983) The Chilean nitrate deposits. *Am Sci* 71: 366-374

590 Faryad SW (2002) Metamorphic conditions and fluid compositions of scapolite-bearing rocks  
591 from the lapis lazuli deposit of Sare Sang, Afghanistan. *J Petrol* 43: 725-747

592 Feneyrol J (2012) *Pétrologie, géochimie et genèse des gisements de tsavorite associés aux*  
593 *gneiss et roches calco-silicatées graphiteux de Lemshuku et Namalulu (Tanzanie)*. Ph.D  
594 Institut National Polytechnique de Lorraine, Vandœuvre-lès-Nancy, France

595 Feneyrol J, Giuliani G, Ohnenstetter D, Le Goff E, Malisa PJ, Saul M (2010)  
596 Lithostratigraphic and structural controls of tsavorite deposits at Lemshuku, Merelani area,  
597 Tanzania. *Contrôles lithostratigraphique et structural des gisements de tsavorite de*  
598 *Lemshuku, région de Merelani, Tanzanie*. *C R Acad Sci* 342: 778-785

599 Feneyrol J, Ohnenstetter D, Giuliani G, Fallick AE, Rollion-Bard CI, Robert JL, Malisa E  
600 (2012) Evidence of evaporites in the genesis of the vanadian grossular tsavorite deposit in  
601 Namalulu, Tanzania. *Can Mineral* 50: 745-769

602 Feneyrol J, Giuliani G, Ohnenstetter D, Fallick AE, Martelat JM, Monié P, Dubessy C,  
603 Rollion-Bard CI, Le Goff E, Malisa E, Rakotondrazafy AFM, Pardieu V, Kahn T, Ichang'i,  
604 D, Venance E, Voarintsoa NR, Ranatsenho M, Simonet C, Omito E, Nyamai C, Saul M  
605 (2013) Worldwide tsavorite deposits: new aspects and perspectives. *Ore Geol Rev* 53: 1-25

606 Fritz H, Abdelsalam M, Ali KA, Bingen B, Collins AS, Fowler AR, Ghebread W,  
607 Hauzenberger CA, Johnson PR, Kusky TM, Macey P, Muhongo S, Stern RJ, Viola G  
608 (2013) Orogen styles in the East Africa region: a review of the Neoproterozoic to  
609 Cambrian tectonic evolution. *J Afr Earth Sci* 86: 65-106

610 Garnier V, Ohnenstetter D, Giuliani G (2004) L'aspidolite fluorée: rôle des évaporites dans la  
611 genèse des marbres de Nangimali (Azad-Kashmir, Pakistan). *C R Acad Sci* 336: 1245-  
612 1253

613 Garnier V, Maluski H, Giuliani G, Ohnenstetter D, Schwarz D (2006) Ar-Ar and U-Pb ages  
614 of marble-hosted ruby deposits from central and southeast Asia. *Can J Earth Sci* 43: 509-  
615 532

616 Garnier V, Giuliani G, Ohnenstetter D, Fallick AE, Dubessy J, Banks D, Hoàng Quang V,  
617 Lhomme Th, Maluski H, Pêcher A, Bakhsh KA, Pham Van L, Phan Trong T, Schwarz D  
618 (2008) Marble-hosted ruby deposits from central and Southeast Asia: towards a new  
619 genetic model. *Ore Geol Rev* 34: 169-191

620 Giuliani G, Cheilletz A, Dubessy J, Rodriguez CT (1993a) Emerald deposits from Colombia:  
621 chemical composition of fluid inclusions and origin. In: Nägele u. Obermiller (eds)  
622 Proceedings of the 8th biennial IAGOD symposium, Ottawa, Canada. pp 159-168

623 Giuliani G, Cheilletz A, Sheppard SMF, Arboleda C (1993b) Geochemistry and origin of the  
624 emerald deposits of Colombia. In: Hach-Ali F, Torres L and Gervilla F (eds) Current  
625 research in geology applied to ore deposits, Proceedings of the 2nd biennial meeting of the  
626 Society for Geology Applied to Mineral Deposits, Granada, Spain, pp 105-108

627 Giuliani G, Cheilletz A, Arboleda C, Rueda F, Carillo V, Baker J. (1995) An evaporitic origin  
628 of the parent brines of Colombian emeralds: fluid inclusion and sulfur isotopic evidence. *Eur*  
629 *J Mineral* 7: 151-165

630 Giuliani G, France-Lanord C, Zimmermann JL, Cheilletz, A, Arboleda C, Charoy B, Coget P,  
631 Fontan F, Giard D (1997) Composition of fluids,  $\delta D$  of channel  $H_2O$  and  $\delta^{18}O$  of lattice

632 oxygen in beryls: genetic implications for Brazilian, Colombian and Afghanistani emerald  
633 deposits. Intern Geol Rev 39: 400-424

634 Giuliani G, France-Lanord Ch, Cheilletz A, Coget P, Branquet Y, Laumonier B (2000)  
635 Sulfate reduction by organic matter in Colombian emerald deposits: chemical and stable  
636 isotope (C, O, H) evidence. Econ Geol 95: 1129-1153

637 Giuliani G, Dubessy J, Banks D, Hoang Quang V, Lhomme T, Pironon J, Garnier V, Phan  
638 Trong T, Pham Van L, Ohnenstetter D, Schwarz D (2003) CO<sub>2</sub>-H<sub>2</sub>S-COS-S<sub>8</sub>-AlO(OH)-  
639 bearing fluid inclusions in ruby from marble-hosted deposits in Luc Yen area, North  
640 Vietnam. Chem Geol 194: 167-185

641 Giuliani G, Groat L, Ohnenstetter D, Fallick AE, Feneysel J (2014a) The geology of gems  
642 and their geographic origin. In: Raeside ER (ed) Geology of Gem Deposits, Mineralogical  
643 Association of Canada, Short Course Series 44, Tucson, USA, pp 113-134

644 Giuliani G, Ohnenstetter D, Fallick AE, Groat L, Fagan J (2014b) The geology and genesis of  
645 gem corundum deposits In: Raeside ER (ed) Geology of Gem Deposits, Mineralogical  
646 Association of Canada, Short Course Series 44, Tucson, USA, pp 29-112

647 Giuliani G, Dubessy J, Banks D, Lhomme Th, Ohnenstetter D (2015a) Fluid inclusions in  
648 ruby from Asian marble deposits: genetic implications. Eur J Mineral 27: 393-404

649 Giuliani G, Ohnenstetter D, Rollion Cl, Feneysel J, Martelat JE, Omito E, Ichang'i D, Nyamai  
650 Ch, Wamunyu A (2015b) The boron isotopic composition of tourmaline from tsavorite  
651 deposits in the Neoproterozoic Mozambique metamorphic belt, with a special focus on the  
652 mining districts in Kenya. In: André-Mayer AS, Cathelineau M, Muchez Ph, Picard E,  
653 Sindern S (eds) From source, transport and metal deposits to mineral resources in a  
654 sustainable world, Proceedings of the 13th biennial meeting of the Society for Geology  
655 Applied to Mineral Deposits, Nancy, France, pp 1319-1322

656 Groat L.A. (2014) Geology of Gem Deposits. Mineralogical Association of Canada Short  
657 Course series 44, Raeside R. (ed), Tucson Arizona, USA

658 Hubbard MS, Grew ES, Hodges KV, Yates MG, Pertsev NN (1999) Neogene cooling and  
659 exhumation of upper-amphibolite-facies 'whiteschists' in the southwest Pamir Mountains,  
660 Tajikistan. Tectonophysics 305: 325-337

661 Hughes R.W. (1997) Ruby and Sapphire, RW Hughes publishing, Boulder, USA

662 Kazmi AH, Snee LW (1989) Emeralds of Pakistan, Van Nostrand Reinhold, New York, USA

663 Kozlowski A, Metz P, Jaramillo HAE (1988) Emeralds from Sodomondoco, Colombia:  
664 chemical composition, fluid inclusion and origin. Neues Jahrbuch Miner Abh 59: 23-49

665 Kulke HG (1974) Die lapis-lazuli Sar-e-Sang (Badakhshan): geologie, entstehung,  
666 kulturgeschete und bergau. Afghanistan Journal: 43-56

667 Kulke HG, Schreyer W (1973) Kyanite-talc schist from Sar e Sang, Afghanistan. Earth Planet  
668 Sci Lett 18: 324-328

669 Lacassagne V, Bessedat C, Florian P, Bouvet S, Olliver B, Coutures JP, Massiot D (2002)  
670 Structure of high temperature NaF-AlF<sub>3</sub>-Al<sub>2</sub>O<sub>3</sub> melts: a multinuclear NMR study. J Phys  
671 Chem 106: 1862-1868

672 Laumonier B, Branquet Y, Cheilletz A, Giuliani G, Rueda F (1996) Les gisements  
673 d'émeraude de Muzo et de Coscuez (ouest de la Cordillère Orientale de Colombie) sont des  
674 duplex formés pendant une phase de tectonique en chevauchement à la limite Eocène-  
675 Oligocène. C R Acad Sci 320: 1171-1178

676 Machel HG, Krouse HR, Sassen R (1995) Products and distinguishing criteria of bacterial and  
677 thermochemical sulphate reduction. Appl Geochem 10: 373-389

678 Mattauer M, Matte Ph, Jolivet JL, (1999) A 3D model of the India-Asia collision at plate  
679 scale: C R Acad Sci 328: 499-508

680 Olivier B (2006) The geology and petrology of the Merelani tanzanite deposit, NE Tanzania.  
681 Ph.D University of Stellenbosch, South Africa

682 Ottaway TL, Wicks FJ, Bryndzia LT, Kyser TK, Spooner ETC (1994) Formation of the Muzo  
683 hydrothermal emerald deposit in Colombia. Nature 369: 552-554

684 Pêcher A, Giuliani G, Garnier V, Maluski H, Kausar AB, Malik RM, Muntaz HR (2002)  
685 Geology and Geochemistry of the Nangimali ruby deposit area, Nanga-Parbat Himalaya  
686 (Azad Kashmir, Pakistan). J Asian Earth Sci 21: 265-282

687 Pokrovski GS, Dubrovinsky LS (2011) The S<sup>3-</sup> ion is stable in geological fluids at elevated  
688 temperatures and pressures. Science 331: 1052-1054

689 Pokrovski GS, Dubessy J (2014) Stability and abundance of the trisulfur radical ion S<sup>3-</sup> in  
690 hydrothermal fluids. Earth Planet Sci Lett 411: 298-309

691 Polovov IB, Vasin BD, Abakumov AV, Rebrin OI, Chernyshov MV, Volkovich VA, Griffiths  
692 TR (2007) Thermodynamics of the formation of vanadium (II) complexes in chloride  
693 melts. In: Mantz RA, Hagiwara M, Trulove HC, De Long H, Stafford GR, Fox D (eds)  
694 "Molten Salts", ECS Transactions" 3, Issue 35, The Electrochemical Society, Pennington,  
695 pp 589-597

696 Reinen D, Lindner GG (1999) The nature of chalcogen colour centres in ultramarine-type  
697 solids. Chem Soc Rev 28: 75-84

698 Roedder E (1963) Studies of fluid inclusions II: freezing data and their interpretation. *Econ*  
699 *Geol* 58: 163-211

700 Sabot B, Cheilletz A, De Donato P, Banks D, Levresse D, Barrès O (2000) Afghan emeralds  
701 face Colombian cousins. *Chron Rech Min* 541: 111-114

702 Samson I, Anderson A, Marshall D (2003) Fluid inclusions: Analysis and interpretation.  
703 Mineralogical Association of Canada, Short Course series 32, Raeside R. (ed), Vancouver,  
704 British Columbia, Canada

705 Schreyer W, Abraham K (1976) Three-stage metamorphic history of a whiteschist from Sar e  
706 Sang, Afghanistan, as part of a former evaporite deposit. *Contrib Mineral Petrol* 59: 111-  
707 130

708 Tapponnier P, Mattauer M, Proust F, Cassaigneau Ch (1981) Mesozoic ophiolites, sutures,  
709 and large-scale tectonic movements in Afghanistan. *Earth Planet Sci Lett* 52: 355-371

710 Tenczer V, Hauzenberger C, Fritz H, Hoinkes G, Muhongo S, Klötzli U (2013) Crustal age  
711 domains and metamorphic reworking of the deep crust in Northern-Central Tanzania: a  
712 U/Pb zircon and monazite age study. *Mineral Petrol* 107: 679-707

713 Truche L, Bazarkina EF, Barré G, Thomassot E, Berger G, Dubessy J, Robert P (2014) The  
714 role of S<sup>3-</sup> ion in thermochemical sulphate reduction: geological and geochemical  
715 implications. *Earth Planet Sci Lett* 396: 190-200

716 Van Hinsberg VJ, Henry DJ, Marschall HR (2011) Tourmaline: an indicator of its host-  
717 environment. *Can Mineral* 49: 1-16

718 Vapnik YE, Moroz I (2001) Fluid inclusions in Panjshir emerald (Afghanistan). In: Noronha  
719 F, Dória A, Guedes A (eds), XVI European current research on fluid inclusions, (ECROFI),  
720 Porto, Portugal, Faculdade de Ciências do Porto, Memoria 7, pp 451-454

721 Vasin BD, Polovov IB, Volkovich VA, Griffiths TR, Berezin AV (2004) Coordination state  
722 of vanadium in chloride melts: an electronic absorption spectroscopy study. In: Mantz RA,  
723 Trulove HC, De Long H, Stafford GR, Hagiwara M, Costa DA (eds) "Molten Salts XIV",  
724 Proceedings of the International symposium, Electrochemical Society, 2004-24, New  
725 Jersey, USA, pp 261-268

726 Warren JK (2006) *Evaporites: Sediments, Resources and Hydrocarbons*. Springer, Berlin,  
727 Germany

728 Williams AE, McKibben MA (1989) A brine interface in the Salton Sea Geothermal system,  
729 California: fluid, geochemical and isotopic characteristics. *Geochim Cosmochim Acta* 53:  
730 1905-1920

731 Wilson WE, Saul JM, Pardieu V, Hughes RW (2009) The Merelani tanzanite mines. Mineral  
732 Record 40: 347-408

733 Wood SA (1992) Theoretical prediction of speciation and solubility of beryllium in  
734 hydrothermal solution to 300°C at saturated vapour pressure: application to  
735 bertrandite/phenakite deposits. Ore Geol Rev 7: 249-278

736 Yardley WB, Cleverley JS (2013) The role of metamorphic fluids in the formation of ore  
737 deposits. In: Jenkin GRT, Lusty PAJ, McDonald I, Smith MP, Boyce AJ, Wilkinson JJ  
738 (eds), Ore Deposits in an Evolving Earth. Geol Soc London, Special Publications 393. doi:  
739 10.1144/SP393.5

740 Yardley WB, Bodnar RJ (2014) Fluids in the continental crust. Geochem Persp Lett 3: 1-127

741

742

743

#### 744 **Figure captions**

745 **Figure 1.** Metamorphic gems. A- Crystal of emerald on pyrite, Chivor mines, eastern  
746 emerald belt, Colombia, 3.9x2.6 cm. Collection MultiAxes. B- Association of emerald and  
747 quartz, Muzo mines, western emerald belt, Colombia. C- Emerald crystals on quartz and  
748 adularia, Panjshir Valley, Afghanistan, 6.6x4.4 cm. Specimen Fine Art Mineral. D- Ruby  
749 crystal associated with flakes of phlogopite in a marble matrix, Minh Tien mine, Luc Yen  
750 mining district, Vietnam, 2x1 cm. E- Nodule, rough and cut of tsavorite from the Tsavolite  
751 mine, Mangare mining district, Voi region, Kenya, diameter of the nodule (on the left) ~ 3.5  
752 cm. F- Association lazurite, carbonate and pyrite from Sar-e-Sang mines, Afghanistan,  
753 8.3x6.2 cm, Specimen Crystal Classics. G- Gem crystal of tsavorite (2 cm across) embedded  
754 in a graphitic gangue with calcite (white), Merelani mines, Arusha district, Tanzania. H- Blue  
755 zoisite, variety tanzanite, Merelani, Arusha district, Tanzania, 8.7x5x3 cm. Collection Marcus  
756 Budil. Photos: A to C, F to H, L.-D. Bayle/le Règne Minéral. Photo D: G. Giuliani. Photo E:  
757 V. Pardieu/GIA.

758 **Figure 2.** Colombian emerald mines (modified from Branquet et al. 2015). A- Simplified  
759 geological map of the Colombian Eastern Cordillera with the location of the main emerald  
760 deposits. Inset is location of Figure 2B. B- Geological map of the Chivor area. All emerald  
761 and gypsum deposits and occurrences are hosted within the upper Guavio Formation.

762 **Figure 3.** Geological features of Cr-V-bearing metamorphic gems formed during the  
763 metamorphism of rocks (black shale-carbonate-sandstone with evaporite intercalations) from

764 carbonate platform successions. Be: beryllium; Al: aluminium; Si: silica; Ca: calcium; Cr:  
765 chromium; V: vanadium. Colombian emerald deposits: a: Mg-limestone; b: emerald-bearing  
766 calcareous C-rich BS; c: sandstone; d: pyritic nodules in siliceous BS; e: siliceous BS. Ruby  
767 in marble from central and south-east Asia: f: quartzite; g: amphibolite; h: mica-bearing  
768 marble; i: pyrite-bearing marble; j: calc-schist and garnet-biotite micaschist; k: ruby-  
769 anhydrite-bearing yellow Mg-marble; l: white dolomite and/or calcite marbles. Tsavorite in  
770 graphitic gneiss and calc-silicates from Tanzania: m: biotite-kyanite gneiss; n: graphitic  
771 gneiss; o: tsavorite-bearing nodules in graphitic gneiss and calc-silicate rocks with anhydrite-  
772 gypsum veinlets or lenses; p: calc-silicate rocks; q: kyanite-graphite gneiss; r: dolomitic  
773 marble with anhydrite levels (modified from Giuliani et al. 2014b).

774 **Figure 4.** A- Geological cross-section through the Chivor emerald deposits, eastern  
775 emerald belt (from Branquet et al. 2015). B- South-eastern field view of the cross-section. C-  
776 Chivor Klein pit. Upper contact of the main breccia level (in black) with albitites (1). The  
777 transport of clasts of albitite (2) within the breccia is marked by tails. D- Oriente deposit.  
778 Polygenic breccia formed by clasts of albitite (Ab) and black shales (Bs), cemented by pyrite,  
779 carbonates and albite. E- Oriente deposit. Carbonate (Cb) -pyrite (Py) -emerald-bearing veins  
780 crosscutting albitite (Ab) showing some remnants of black shale (Bs). The greyish tracks  
781 parallels to the carbonate veins are residues of dust not cleaned by the water jet in the mine.  
782 Photos B to D: Y. Branquet and Photo E: G. Giuliani.

783 **Figure 5.** Geological map of the Tequendama and Quipama mines, Muzo mining district,  
784 western emerald belt. U1 through U4 represent the different tectonic units. The cross-section  
785 A-B is drawn on figure 6. Modified from Laumonier et al. (1996).

786 **Figure 6.** Cross-section of the Tequendama mine located at the northern part of the Muzo  
787 emerald mining district (A-B section as shown on Figure 5). The deposit is linked to tear  
788 faults and associated thrusts which are marked by the overlying of the siliceous black shales  
789 by the carbonated ones. The thrust planes are underlined by a hydrothermal breccia (called  
790 "cenicero" by the miners) and hydraulic fracturing. The fluid circulation induced intense  
791 albitisation, carbonatisation and pyritisation of the surrounding black shales (modified from  
792 Branquet et al. 1999b).

793 **Figure 7.** Hydraulic fracturing breccia of black shale located in the tear fault of Coscuez  
794 mine, western Colombian emerald belt. Photo: Y. Branquet.

795 **Figure 8.** Location of the Panjshir emerald and Sar-e-Sang lapis-lazuli deposits in  
796 Afghanistan, and ruby-hosted marble from central and south-east Asia. The main tectonic  
797 structures and blocks are reported from Mattauer et al. (1999): CF: Chaman fault, GF:  
798 Gaoligong fault, SF: Sagain fault, RRF: Red River fault, HK: Hindu Kush, K: Kohistan, P:  
799 Pamir.

800 **Figure 9.** (A) Tectonic map of Kenya and Tanzania (modified after Fritz et al. 2013) with  
801 the localities of the main tsavorite and tanzanite deposits. (B) Tectonic map of Madagascar  
802 (modified after Fritz et al. 2013) with the locality of the tsavorite deposits. (C) Geological  
803 sketch map of SE Kenya and NE Tanzania (modified after Tenczer et al. 2013) with the  
804 localities of the tsavorite and tanzanite. ANS: Arabian Nubian Shield; EG: Eastern Granulite;  
805 WG: Western Granulite.

806 **Figure 10.** Tsavorite mineralisation from the Neoproterozoic Metamorphic Mozambique  
807 Belt in southeastern Kenya and northeastern Tanzania. A- Calc-silicates band (Csb) hosting  
808 diopside (Di) nodules in the graphitic gneiss (Grg) from the Davis Mine, Lualenyi mining  
809 district, Mgama ridge, Kenya. B- Nodule of anhydrite (Anh) and green grossular (Grs-  
810 tsavorite) presenting a 'chicken-wire' texture in a matrix composed of quartz (Qtz) and calcite  
811 (Cal). The nodules are at the contact with the graphitic gneiss (Grg) which have  
812 accumulations of graphite (Gr). Classic mine, eastern part of the Mgama ridge, Kenya. C-  
813 Tsavorite is hosted by meta-evaporitic horizons intercalated in the graphitic gneiss (Grg). The  
814 anhydrite-bearing level (Anh) is formed by nodules showing enterolithic textures and the  
815 anhydrite-alunite (Sulph) level. D- Tsavorite-bearing nodule from the Komolo mine, south of  
816 Arusha, northeastern Tanzania. The nodule is zoned and the mineral assemblages are, from  
817 the centre to the periphery: (i) V- green grossular in the centre (Grs); (ii) the first rim (R1) is  
818 formed predominantly by anhydrite (Anh) + gypsum (Gp), quartz and minor V-titanite, V-  
819 zoisite and small crystals of tsavorite; (iii) the second rim (R2) contains anhydrite (Anh) +  
820 gypsum, clay and minor V-free zoisite; and (iv) the external zone is the graphitic gneiss (Grg)  
821 with quartz, plagioclase, K-feldspar, V-kyanite, V-muscovite, V-rutile, graphite (Gr), F-rich  
822 phlogopite (Phl) and minor calcite and jarosite. Photographs A to C: G. Giuliani; D: J.  
823 Feneyrol.

824 **Figure 11.** SEM images showing the presence of sulphate and salt inclusions in the gems  
825 or associated minerals. A- Ruby (Crn) in equilibrium with dolomite (Dol) formed from the  
826 reaction of spinel (Sp) with calcite. Spinel is a pre-ruby phase which contains high Cr (up to  
827 19 wt. %) and Zn contents (10 wt. %). Spinel is associated with anhydrite (Anh). Hunza

828 Valley, Pakistan. B- The nodule of tsavorite shows remnants of barite (Brt) substituted by  
829 diopside (Di), titanite (Ttn) and tsavorite (Ts), Mine of Nadan 1, Voi region, Kenya. C- Halite  
830 crystal (NaCl) in ruby (Crd). Mine of Jegdalek (Afghanistan). D- Crystals of anhydrite (Anh)  
831 associated with phlogopite (Phl) included in a ruby (Crd) from the Nangimali deposit, Azad  
832 Kashmir, Pakistan. E- Mixtures of salts (Ca-Na-K-[Cl] and sylvite (KCl) found in ruby (Crd)  
833 from the deposits of Luc Yen, Vietnam. F- Anhydrite (Anh) inclusion associated with F-  
834 tremolite (F-Tr) and dolomite (Dol) in marble, Namalulu tsavorite deposit, south of Arusha,  
835 northern Tanzania. G- Tainolite (Tnl) associated with calcite (Cal) in a dolomite (Dol) lens  
836 from the Namalulu tsavorite deposit.

837 **Figure 12.** Parental fluids of emerald, ruby and tsavorite. A- Tabular fluid inclusion  
838 trapped by a Colombian emerald (Chivor mine, eastern emerald belt). The primary cavity  
839 contains a liquid (L), vapour (V), two cubes of halite (H) and a minute crystal of calcite (Cal).  
840 B- Fluid inclusion in a Colombian emerald showing three cubes of halite (H), the liquid phase  
841 (L), the contracted vapour phase (V), a minute black phase (S) and a thin rim of liquid carbon  
842 dioxide (L<sub>1</sub>) rim visible at the bottom part of the vapour phase. C- Multiphase primary fluid  
843 inclusions trapped by an emerald from the Panjshir Valley (Afghanistan). The cavity contains  
844 a vapour (V) and liquid (L) phases, a cube of halite (H), usually a primary and rounded salt of  
845 sylvite (Syl) and aggregates of several unidentified anisotropic grains (S). D- Primary  
846 polycrystalline fluid inclusions trapped by the Mogok ruby in marble from Myanmar. The  
847 cavity contains different solids which are mixtures of carbonates, with Ca-Na-Al cations such  
848 as calcite (Ca), dawsonite (Dw), shortite (Sh), and apatite (Ap), fluorite (Fl), halite (H),  
849 graphite and a CO<sub>2</sub>-H<sub>2</sub>S-bearing fluid phase (CO<sub>2</sub>). E- Primary multiphase H<sub>2</sub>S-dominated FI  
850 (liquid [L<sub>H<sub>2</sub>S</sub>] + vapour [V<sub>H<sub>2</sub>S</sub>]) with native sulphur (S<sub>8</sub>), phengite (Phg) and calcite (Cal) in a  
851 tsavorite from Merelani. Photos: G. Giuliani.

852 **Figure 13.** Origin of salinity in the emerald and quartz-related brines from Colombia and  
853 Afghanistan. A- Analyses of the fluid inclusions from both emerald and quartz show a wide  
854 range of Na/Br and Cl/Br molar ratios that are much greater than those of primary halite and  
855 indicate a substantial loss of Br, typical of recrystallised halite for both emerald deposits. B-  
856 Log(I/Cl) versus Log(Br/Cl) molar ratios of Afghan and Colombian fluid inclusions which are  
857 depleted in both Br and I, indicative of evaporites contribution to the fluids in emerald and  
858 quartz. They are compared with composition of fluids where evaporites are known to be  
859 involved such as for the Salton Sea geothermal brines (Williams and McKibben 1989) and  
860 Hansonburg (Bohlke and Irwin 1992).

861 **Figure 14.** Diagram log (K/Na) molar ratio versus 1/T (°K) showing the evolution of the  
862 fluids associated with Colombian and Afghan emeralds relatively to crustal fluids including  
863 bittern brines, brines derived by dissolution of evaporites, and magmatic fluids (modified  
864 from Yardley and Bodnar 2014). Sedimentary formation brines deviate significantly from the  
865 K-feldspar-albite equilibrium as well as for Afghan and Colombian brines which are  
866 associated with a huge albitisation of their host-rock with the complete consumption of K-  
867 feldspar from respectively, the schist and black shale.

868 **Figure 15.** Boron isotopic composition of tourmalines associated with tsavorite from  
869 Kenya, Tanzania and Madagascar. The  $\delta^{11}\text{B}$  (‰) of tourmalines clearly involves continental  
870 evaporitic material (Feneyrol 2012). The boron isotopic ranges of other Kenyan tourmalines  
871 associated with different rocks from the tsavorite-bearing metasedimentary series are reported  
872 for comparison (Giuliani et al. 2015b). The different boxes representative of different  
873 geological environments are from Barth (1993) and van Hinsberg et al. (2011).

874 **Figure 16.** The formation of metamorphic tsavorite-bearing nodules in a closed  
875 metamorphic system (from Feneyrol et al. 2013). A- The sedimentary nodule is initially an  
876 anhydrite concretion within the silica-rich shales. These shales contained V(-Cr)-rich clays  
877 and organic matter. B- At the beginning of the prograde metamorphism, the host shales turned  
878 into schists, and V(-Cr)-rich clays and organic matter transformed into respectively V(-Cr)-  
879 rich micas and graphite. For the formation of tsavorite, Si and Al came from the schist, V and  
880 Cr from the clays and/or organic matter, and Ca from the anhydrite following the equation:  
881  $3\text{CaSO}_4 + 2\text{Al}^{3+} + 3\text{SiO}_2 + 6\text{H}_2\text{O} \rightarrow \text{Ca}_3\text{Al}_2(\text{SiO}_4)_3 + 6\text{O}_2 + 3\text{H}_2\text{S} + 6\text{H}^+$ .  
882  $\text{H}_2\text{S}$  is trapped by the fluid inclusion cavities in tsavorite. The sulphur is expelled into the  
883 schist to form pyrite. C- At the end of the prograde metamorphism, most of the anhydrite has  
884 been replaced by tsavorite which is also present as small crystals scattered in the evaporitic  
885 rims of the nodule. Pyrite, graphite and V(-Cr)-poor mica are the main minerals present in the  
886 surrounding gneiss.

887

#### 888 **Table caption**

889 **Table 1.** Reconstruction composition of emerald-related fluids from the Panjshir deposits,  
890 Afghanistan (this work). For comparison are reported the composition of the fluids associated  
891 with Colombian emeralds (Banks et al. 2000).

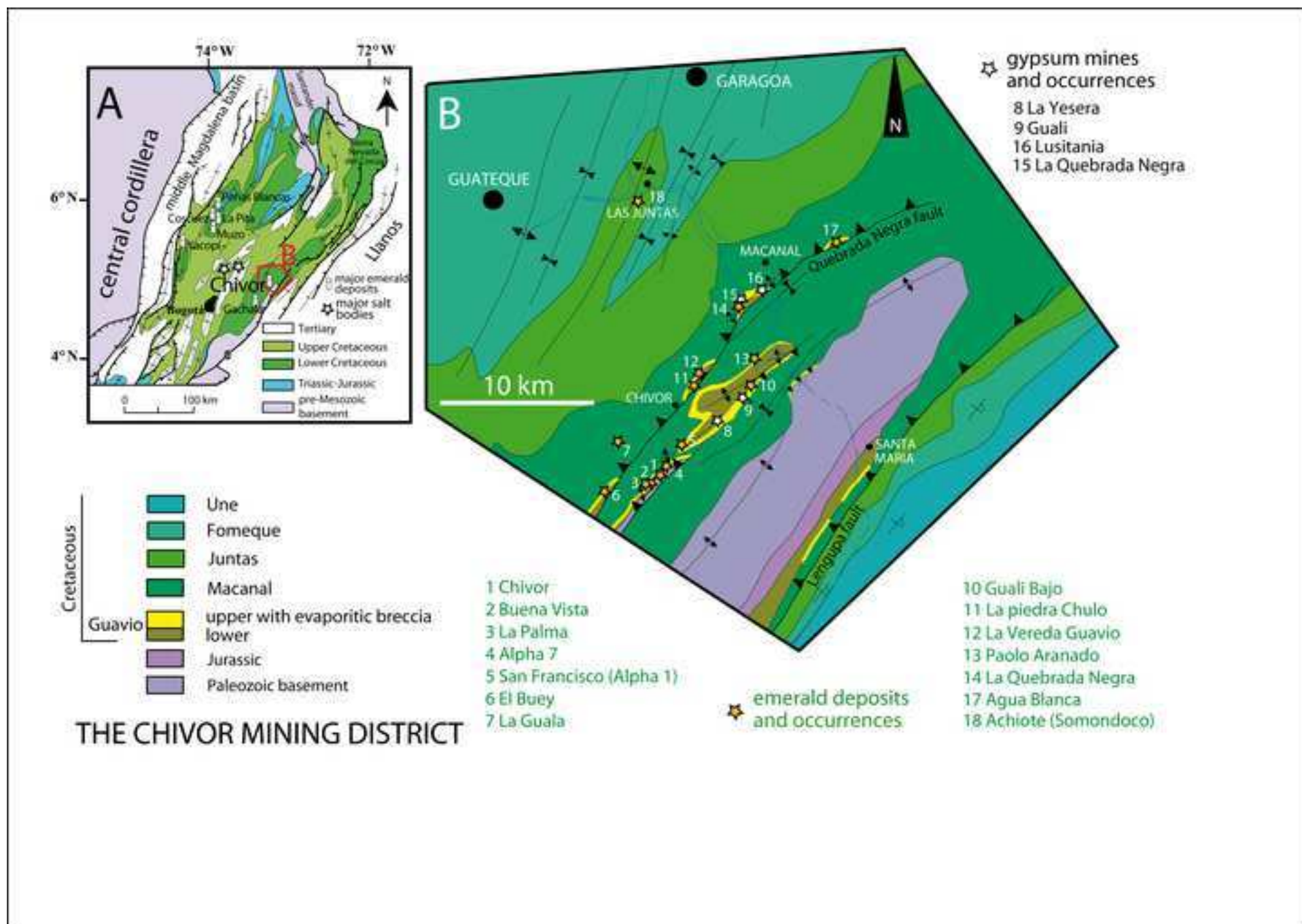
892

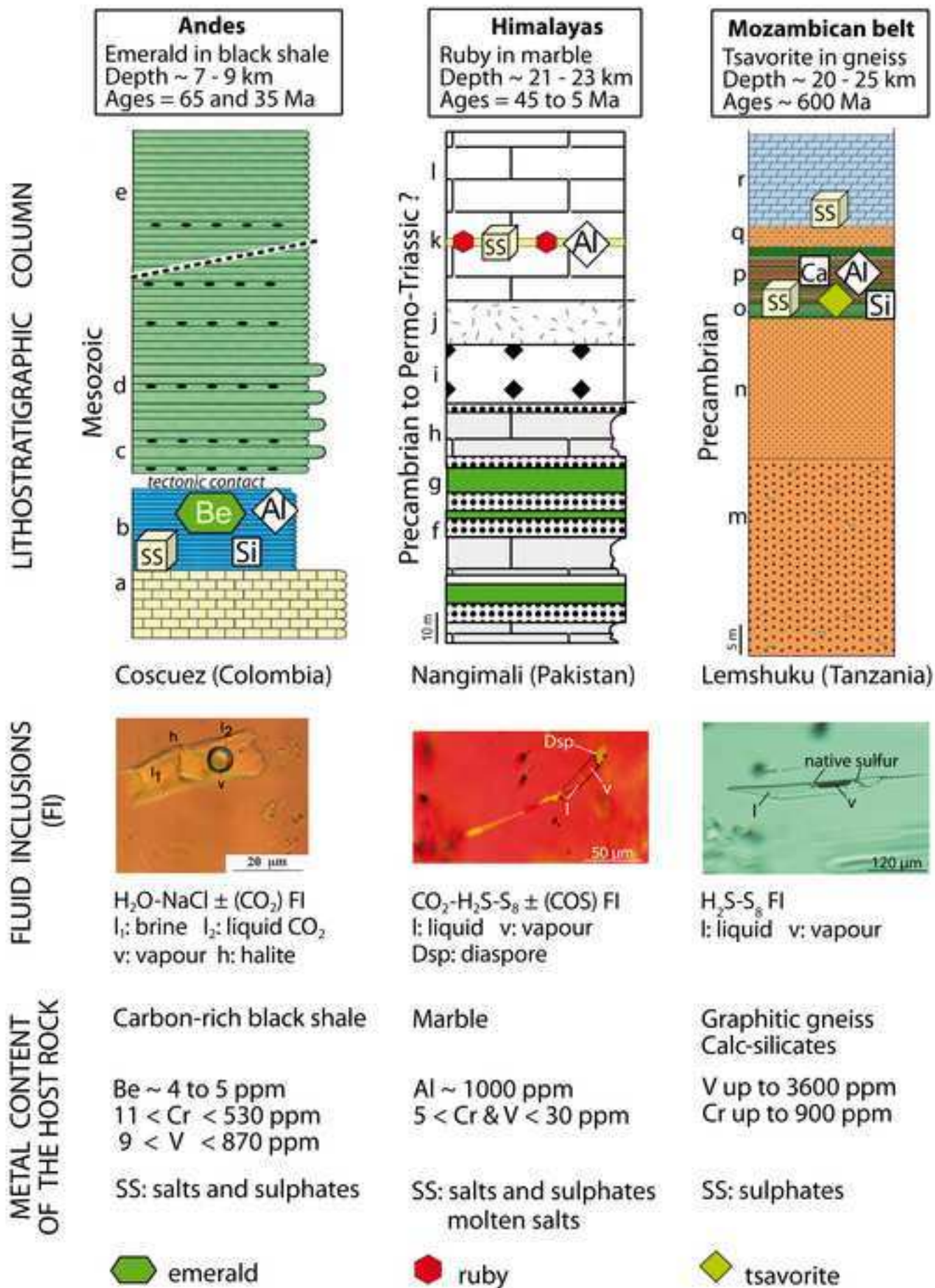
Table

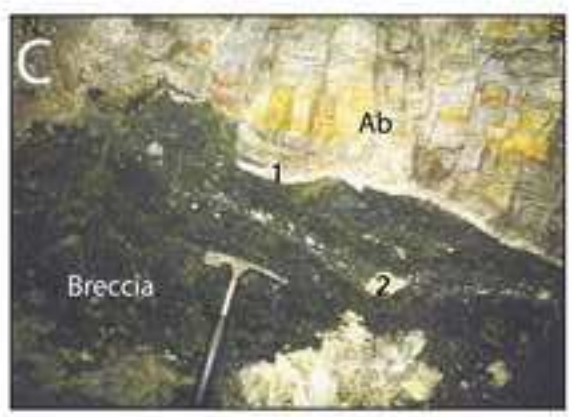
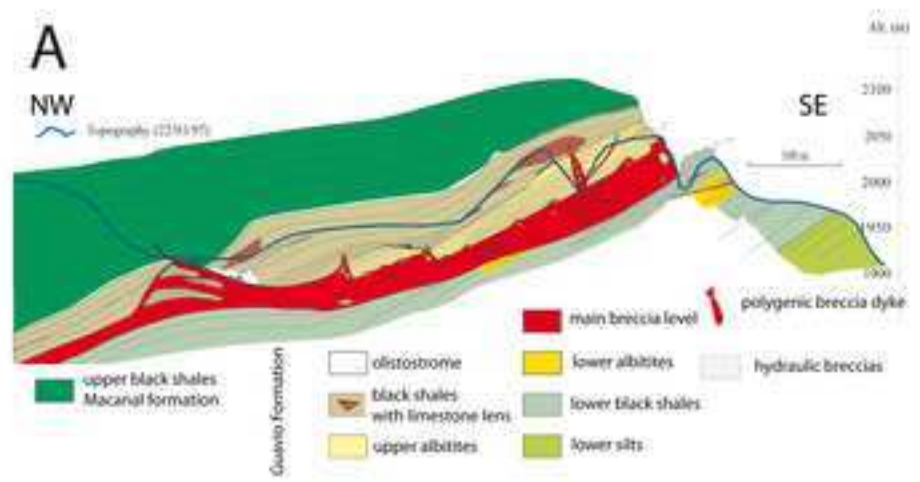
country	deposit	mineral	salinity (wt% eq. NaCl)	Na	K	Li	F (ppm)	Cl	Br	SO <sub>4</sub>	I	Na/K (m)	Na/Br (m)	Cl/Br (m)	Na/Li (m)	Cl/SO <sub>4</sub> (m)	og(Br/Cl)log(I/Cl) (m)	
<b>AFGHANISTAN</b>																		
	Kendjt	quartz	34	103.711	25.250	171	118	206.310	44.2	147	0.29	6.98	8152.12	10520.63	182.55	3792.17	-4.02	-6.40
	Kendjt	"	34	107.729	26.800	180	115	206.310	36.4	143	0.31	6.83	10286.9	12780.53	180.24	3905.72	-4.11	-6.38
	Kendjt	emerald	34	78.205	34.062	207	670	206.310	41.4	4310	0.49	3.9	6563.65	11233.31	114.02	129.63	-4.05	-6.18
	Butizor	"	34	97.257	22.573	220	nd	206.310	20	1058	0.8	7.32	16928.4	23296.37	133.67	528.13	-4.37	-5.97
	Gujari	"	34	72.325	30.322	261	nd	206.310	39.8	1331	0.41	4.05	6311.74	11680.32	83.68	419.57	-4.07	-6.25
	Shigar	"	34	71.969	29.692	245	nd	206.310	41.2	824	0.52	4.12	6065.24	11279.71	88.73	677.63	-4.05	-6.16
<b>COLOMBIA*</b>																		
	Yacopi	emerald	38	100.376	22.585		nr	224.007	80.2	6491	4.5	7.56	4347.85	6294.79		93.45	-3.80	-5.25
	Coscuez	"	38	130.946	5795	944	nr	230.082	36.7	463	0.3	0.04	12395	14128.97	41.86	1345.61	-4.15	-6.44
	Cincho	"	37	94.823	18.813	1261	nr	224.306	39.7	166	1.9	8.57	8297.40	12733.39	22.69	3658.9	-4.10	-5.63
	Palo Aranado	"	40	122.677	8829	1165	nr	242.43	55.5	232	0.68	0.02	7678.72	9844.35	31.77	2829.55	-3.99	-6.11
	Oriente	"	38	116.142	5888	430	nr	230.202	27.4	352	0.36	0.03	14725.1	18934.43	81.5	1770.86	-4.28	-6.36
	Klein	"	40	98.923	10.248	1959	nr	240.698	51.0	1966	2.61	16.41	6738.23	10636.44	15.24	331.52	-4.03	-5.52
	Yacopi	quartz	40	94.019	19.556		nr	240.815	328.1	1567	0.9	8.17	995.47	1654.14		416.13	-3.22	-5.98
	Coscuez	"	35	54.590	11.622	2031	nr	211.091	100.6	1189	0.2	7.99	1885.10	4728.96	8.11	480.74	-3.67	-6.58
	Coscuez	"	41	106.484	14.833		nr	248.415	118.4	238	0.9	12.20	3124.29	4728.46		2826.31	-3.67	-5.99
	Coscuez	"	42	92.542	10.467	2212	nr	254.132	65.8	658	3	15.03	4885.76	8704.17	12.62	1045.81	-3.94	-5.48
	Cincho	"	39	63.557	11.567	4322	nr	230.481	99.0		1.6	9.34	2230.22	5246.79	4.44		-3.72	-5.71
	Cincho	"	41	103.599			nr	247.813	390	558	5		922.80	1432.03		1202.56	-3.16	-5.25
	Pava	"	41	110.776	5449	432	nr	227.371	150.7	24	2.7	0.03	2553.59	3400.29	77.37	25653.2	-3.53	-5.48
	Oriente	"	31	76.239	12.389		nr	188.233	87.7	997	3.1	10.46	3019.93	4837.15		511.23	-3.68	-5.34
	Klein	"	31	68.344	8796	2549	nr	183.208	42.8		1.5	0.01	5547.22	9647.05	8.09		-3.98	-5.64
	Guali	"	40	78.554	17.415	2090	nr	242.078	23.8	614	2.2	7.67	11466	22923.04	11.34	1067.59	-4.36	-5.60

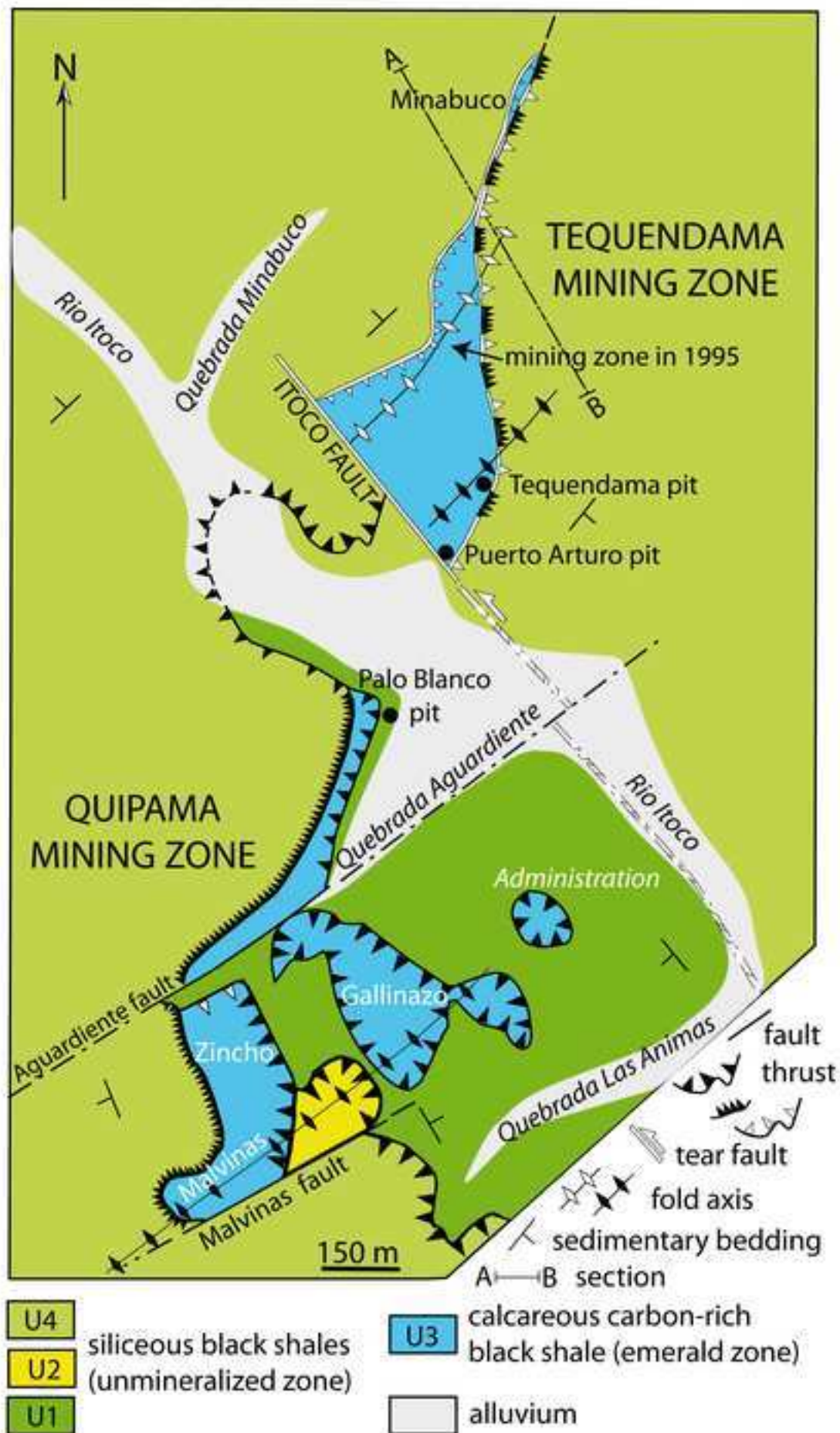
nd: not detected; nr: not reported because measured at the limit of detection (~ 1ppm); \* Banks et al. (2000)

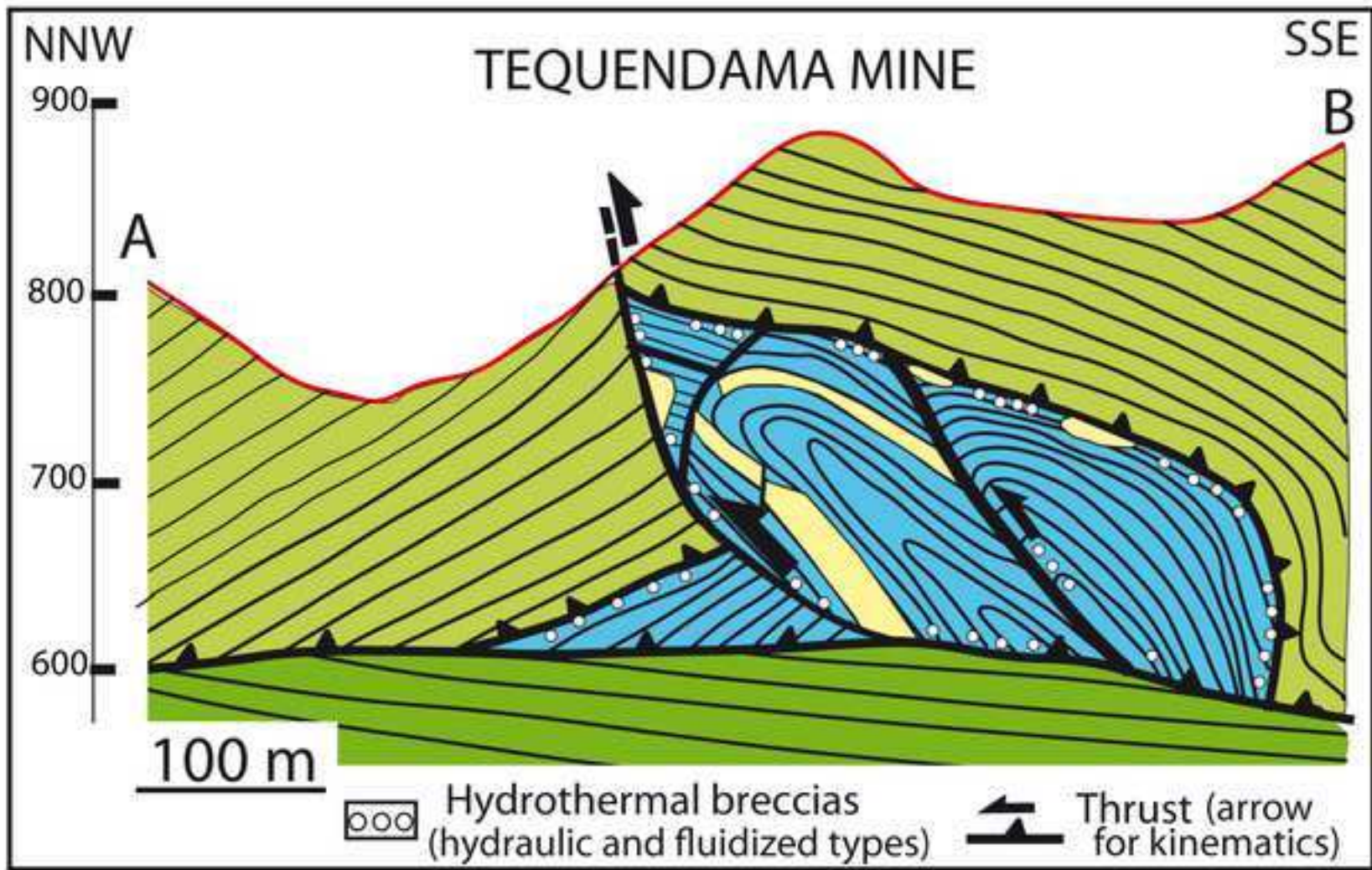






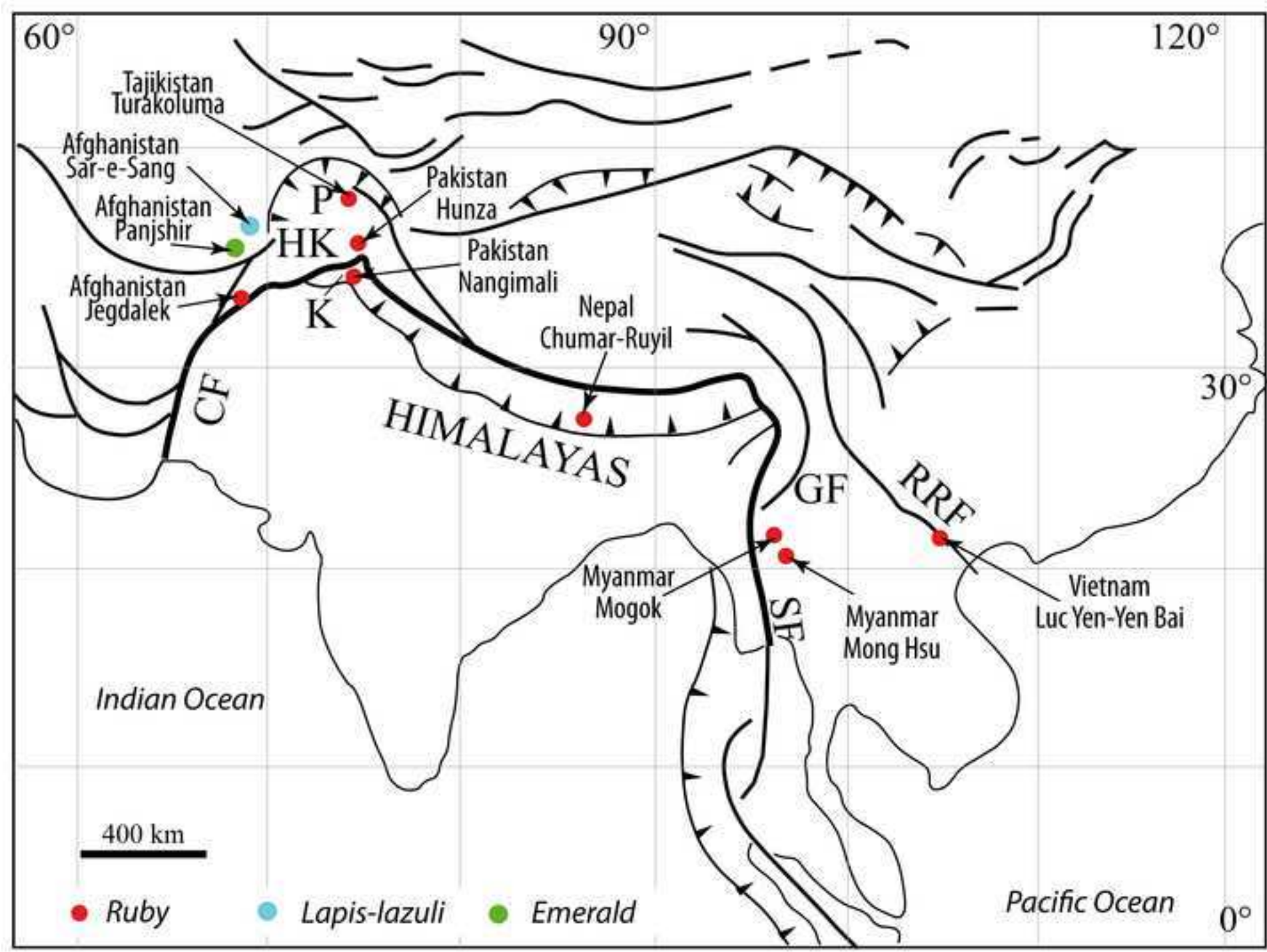


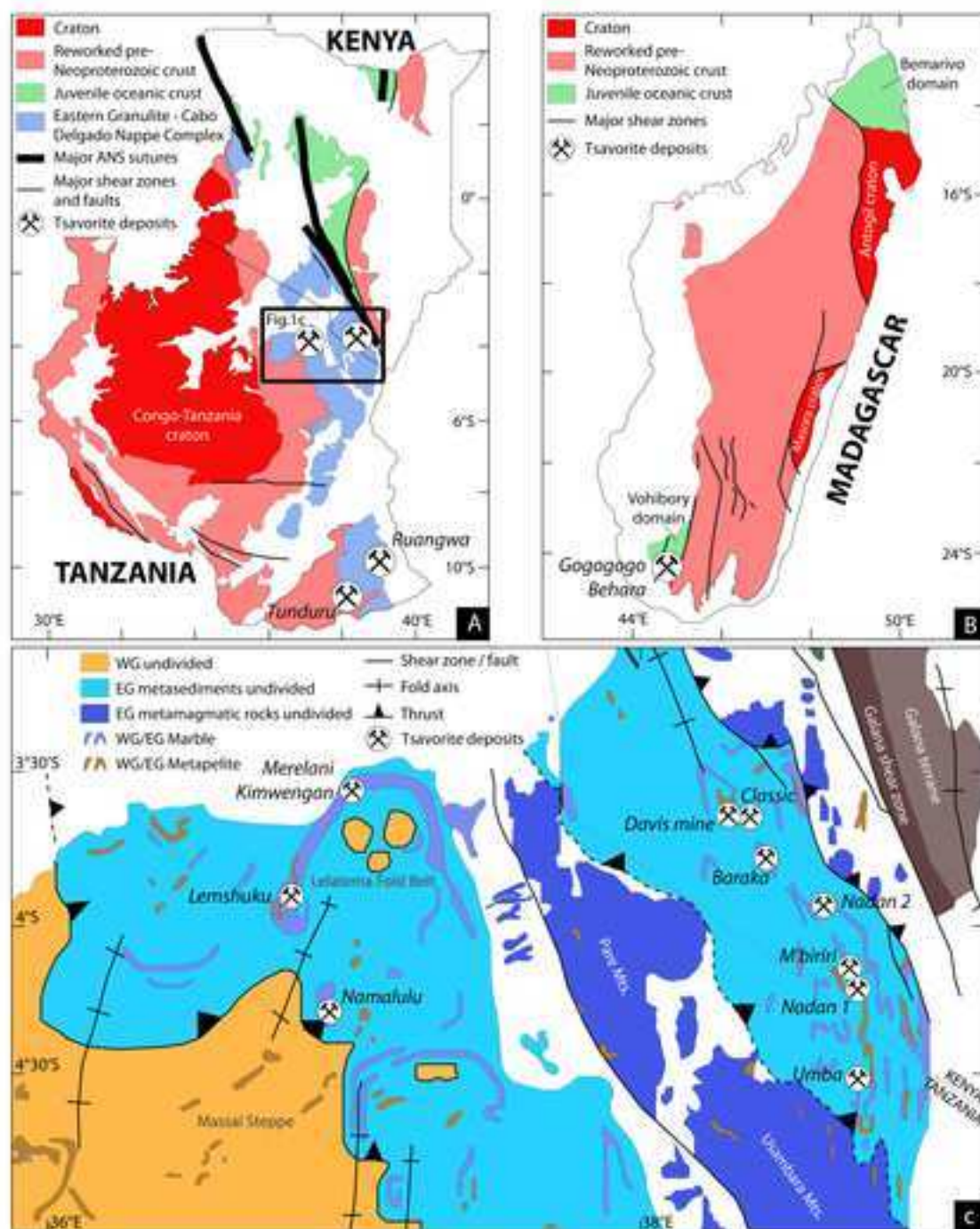


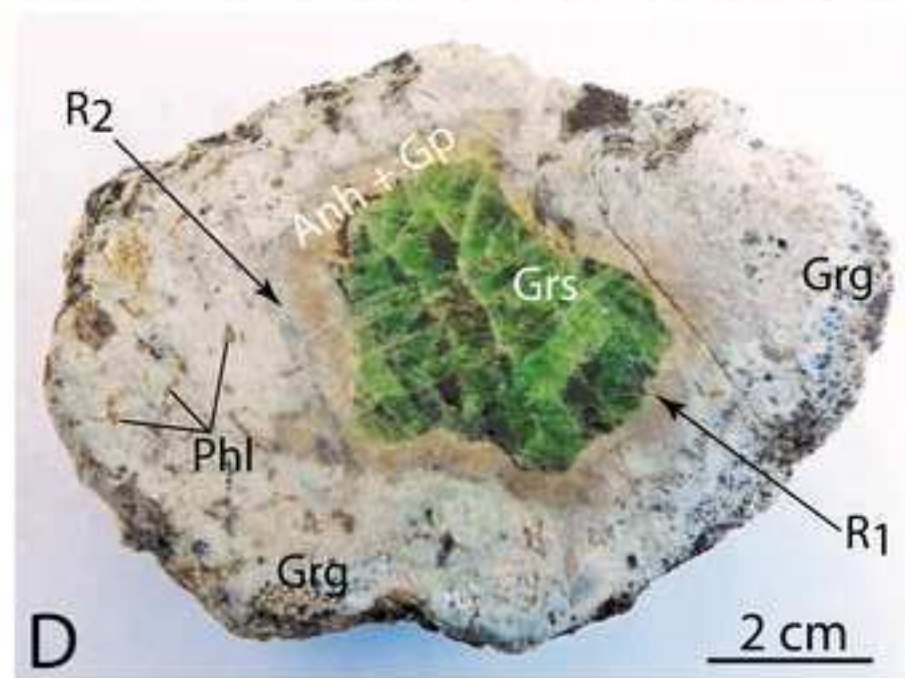
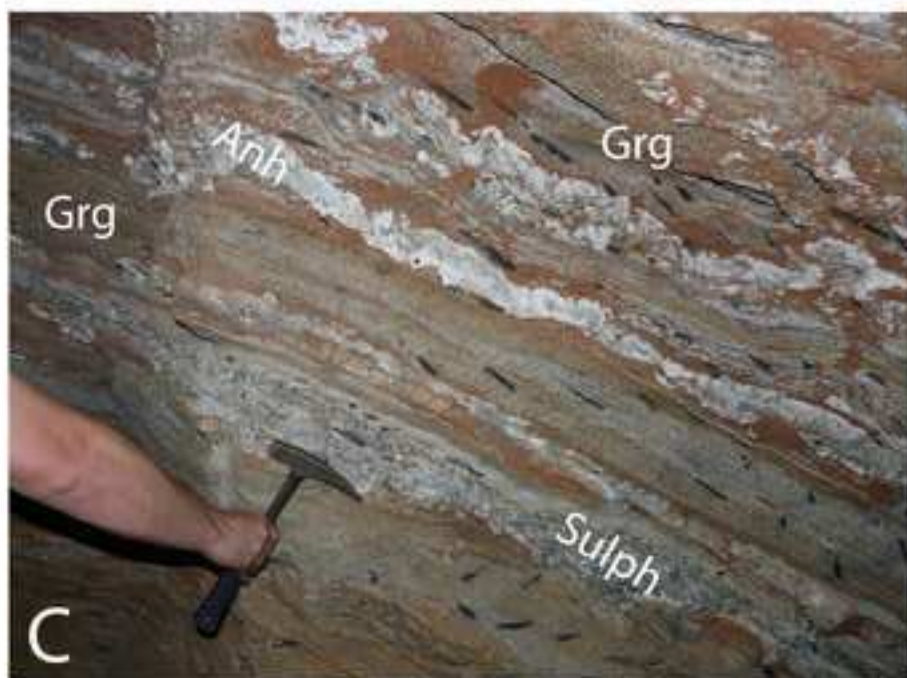
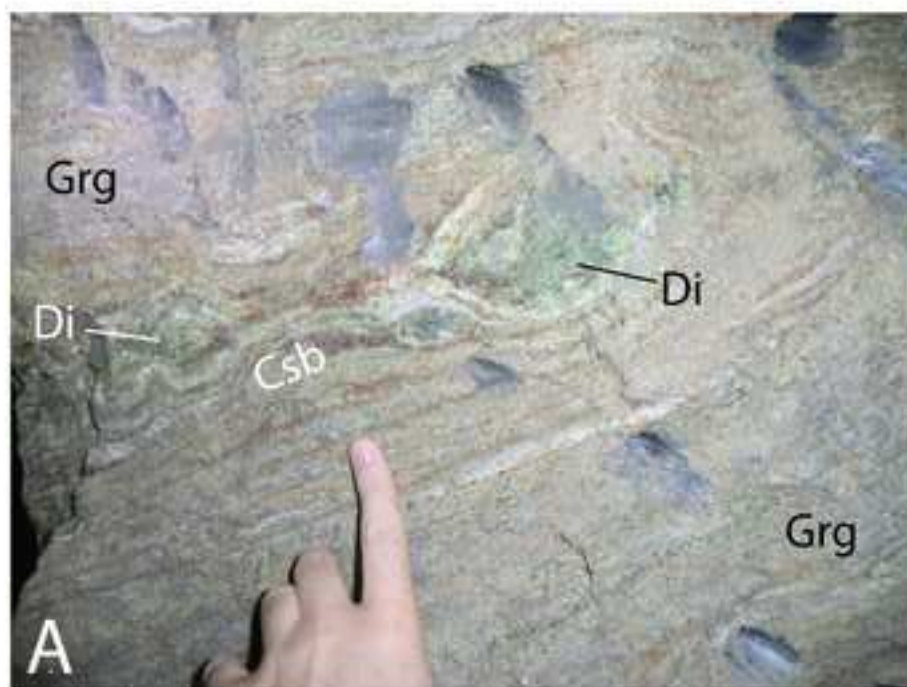


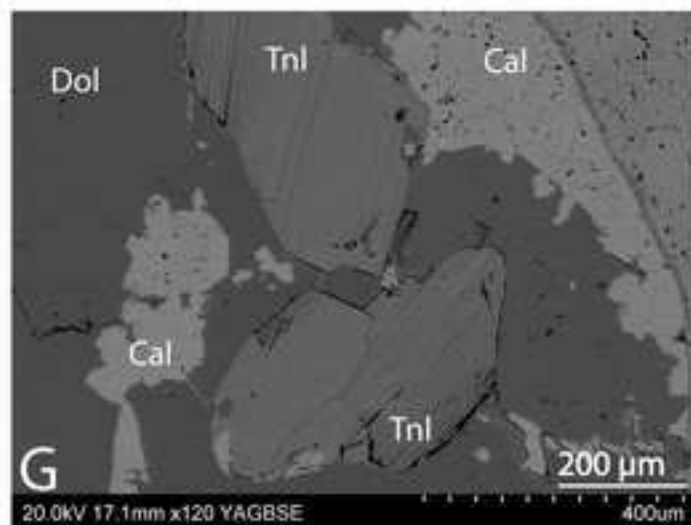
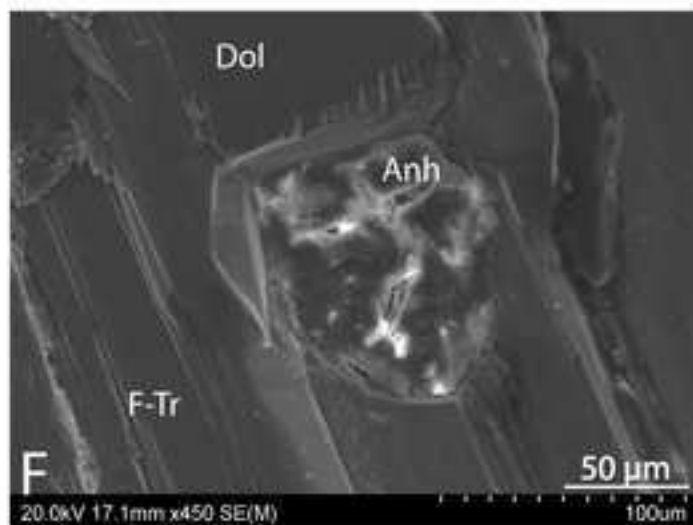
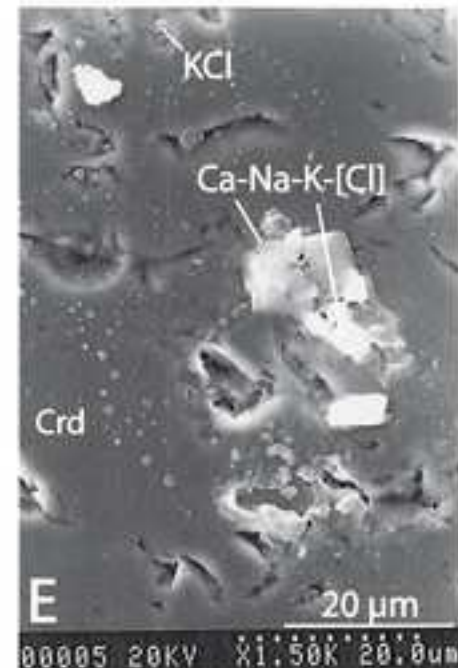
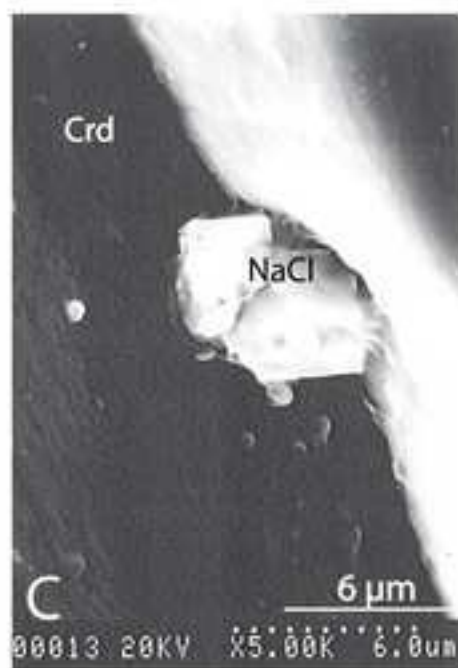
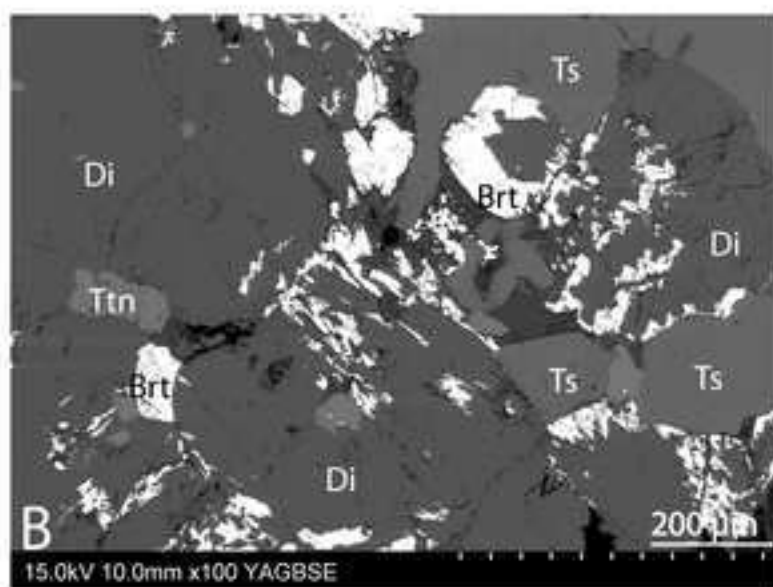
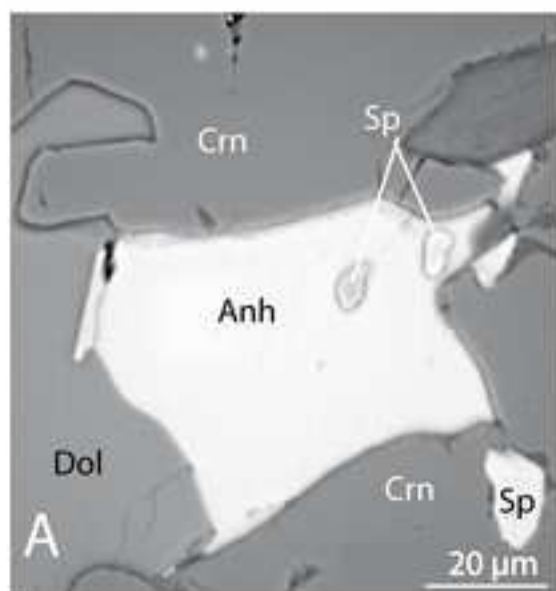
- ↑  siliceous black shales (permeability barrier)
-  carbonated black shale (fluid-saturated rock mass)
-  albitites

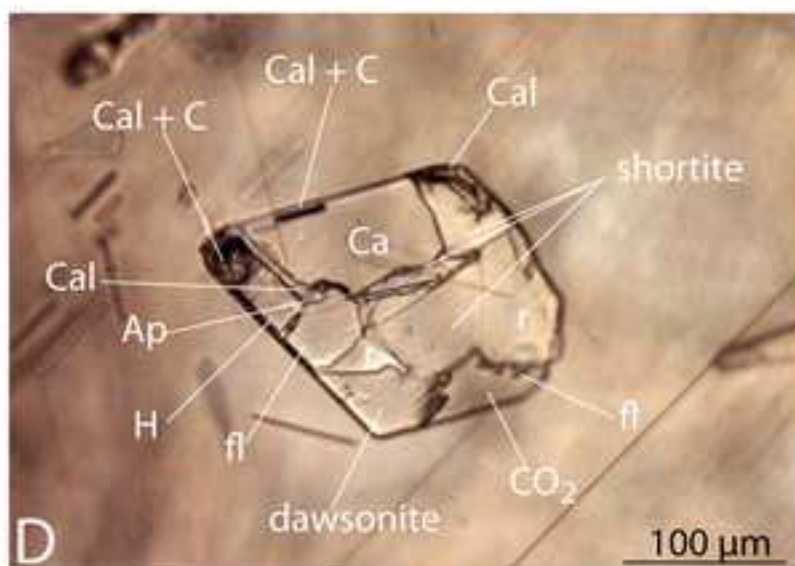
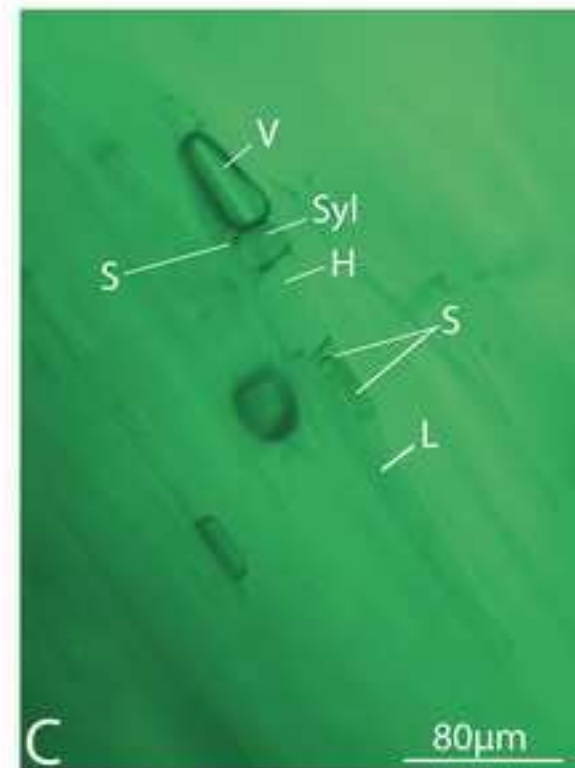
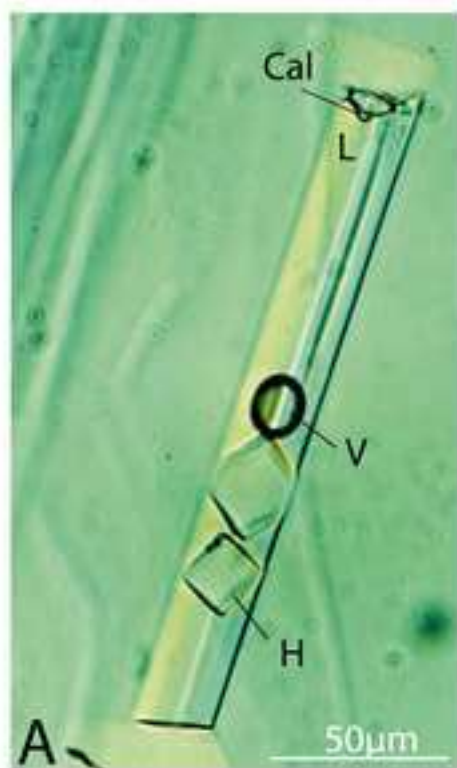


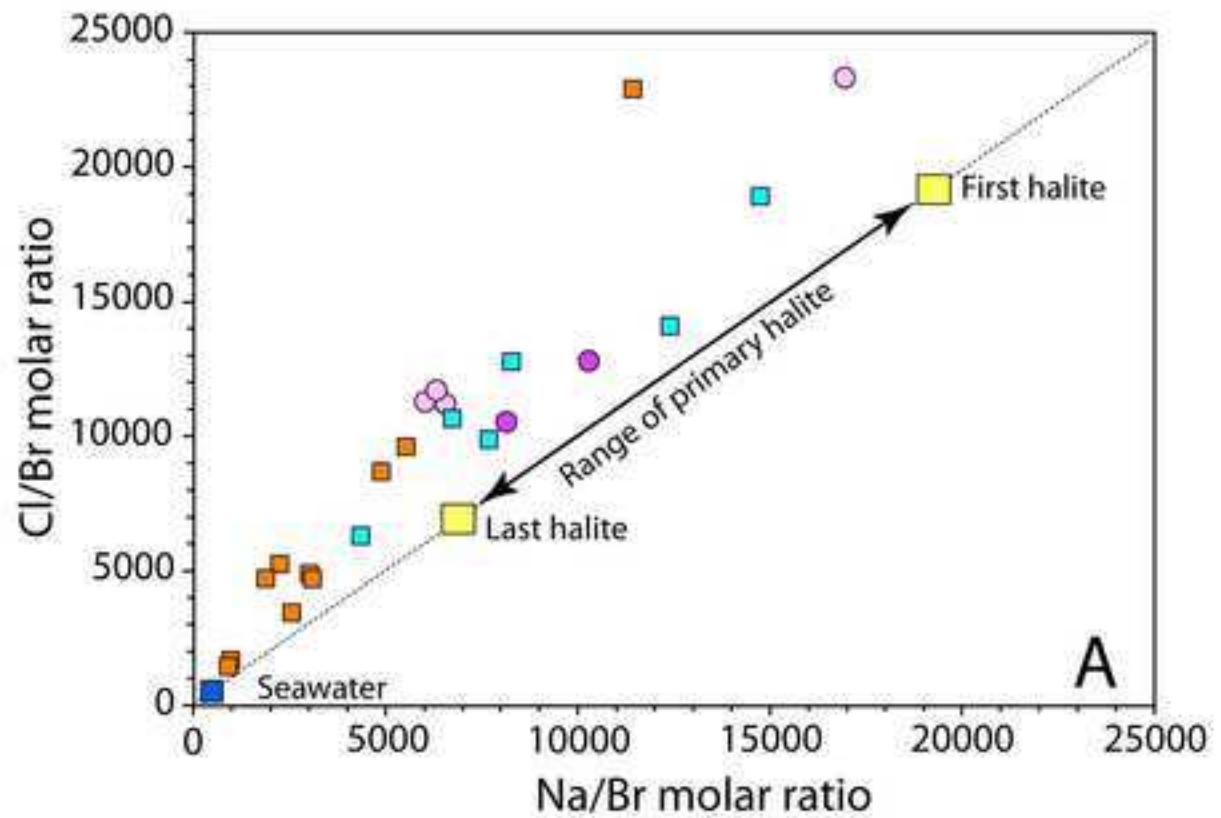












Afghanistan

● quartz

● emerald

Colombia

■ quartz

■ emerald

